UNITED STATES DEPARTMENT OF THE INTERIOR

GEOLOGICAL SURVEY

Vertical Seismic Profiles at the Multi-well Experiment Site, Garfield County, Colorado

By

Myung W. Lee[1]

Open-File Report 84-168

[1]U.S. Geological Survey, Box 25046, Denver Federal Center, Denver, Colorado 80225

1984

TABLE OF CONTENTS

	Page
Abstract	1
Introduction	1
Acknowledgments	2
Field procedure	2
Processing	2
Near-offset VSP data	5
Far-offset VSP data	15
Discussion of data	29
Interpretation	31
Identification of reflected events	31
Seismic characters	37
Acoustic parameters	47
Summary and conclusions	50
Recommendations	53
References Cited	53

ILLUSTRATIONS

Figure	1.	VSP field layout at MWX well site near Rifle, Colorado	3
	2.	General processing flow sheet for the vertical component, near-offset VSP data	6
	3.	Raw VSP data at MWX 2 well from the near-offset source	7
	4.	Monitor-phone record at the well-phone depth level of 7,025 ft	8
	5.	Monitor-phone record at the well-phone depth level of 3,025 ft	9
	6.	Near-offset, vertical component VSP data at MWX 2 well	10
	7.	Downgoing waves of figure 6	11
	8.	Upgoing waves of figure 6	12
	9a.	Downgoing wave at the depth level of 3,025 ft	13
	9b.	Downgoing wave at the depth level of 3,025 ft after downgoing wave deconvolution	14
	10.	Cumulative-summed, vertical-component upgoing waves at MWX 2 well	16
	11.	General processing flow sheet for the three-component, far-offset VSP data at MWX 2 well	18
	12.	Diagram showing particle motion, reference coordinate system and local coordinate system	19
	13a.	Example showing the effect of orientation of horizontal-component VSP data at MWX 2 well	21
	13b.	Example showing the effect of orientation of horizontal-component data at MWX 2 well	22
	14.	Schematic raypath diagram for a dynamic time correction	23
	15.	Schematic raypath diagram for a multi-layered media	25

16. Comparison between unprocessed and processed far-offset VSP data at MWX 2 well---------- 30
17. Cumulative-summed, vertical-component upgoing waves at MWX 2 well after the second downgoing wave deconvolution---------- 32
18. In-line, horizontal-component data at MWX 2 well from the far-offset source---------- 33
19. Cumulative-summed, vertical-component upgoing waves at MWX 2 well from the near-offset source-- 34
20. Merged downgoing and upgoing waves at MWX 2 well from the near-offset source---------- 35
21. Cumulative-summed, vertical-component upgoing waves at MWX 2 well from the far-offset source--- 36
22. SH-waves at MWX 2 well from the far-offset source----- 38
23a. One-dimensional seismic modeling for the coal beds in the paludal zone at MWX 2 well (25 Hz)-------- 39
23b. One-dimensional seismic modeling for the coal beds in the paludal zone at MWX 2 well (80 Hz)-------- 40
24. Vertical-component upgoing wave at MWX 1 well from the near-offset source with various band-pass filters---------- 41
25. Vertical-component upgoing wave at MWX 2 well from the near-offset source with various band-pass filters---------- 42
26. Vertical-component upgoing wave at MWX 2 well from the far-offset source with various band-pass filters---------- 44
27. Correlation between P- and SH-wave at MWX 2 well------ 45
28. Detailed correlation between P- and SH-wave at MWX 2 well from the far-offset source---------- 46
29. Estimated acoustic parameters at MWX 2 well from the far-offset VSP data---------- 48
30. The variation of the percentage error in estimating Poisson's ratio---------- 49
31. The variation of the percentage error in estimating the bulk density using tube-wave velocities------ 51
32. Downgoing wave at MWX 2 well at the depth level of 7,775 ft after downgoing-wave deconvolution--- 52

TABLES

Table 1. Channel distribution of MDS 10 recording system for the VSP experiment at MWX well site, Garfield County, Co.---------- 4

VERTICAL SEISMIC PROFILES AT THE MULTI-WELL EXPERIMENT SITE, GARFIELD COUNTY, COLORADO

By Myung W. Lee

ABSTRACT

The U.S. Geological Survey conducted a vertical seismic profile (VSP) experiment at the Department of Energy Multi-Well Experiment (MWX) site during May 1982. The primary purpose of this experiment was to correlate high-resolution, 3-D surface seismic data with well logs using the vertical seismic data. Additionally, the vertical seismic data were to be evaluated as a seismic tool in determining the lateral extent of lenticular-type sand bodies in this area.

Two wells were profiled with a tri-axial, three-component downhole geophone and a 450 $in.^3$ surface airgun source at two locations. In addition to longitudinal VSP data, very reliable shear VSP data were recorded from the far-offset source. Longitudinal and shear-wave reflections were extracted, and analysis of reflection character indicates that shear wave may have higher resolution capability in detecting lenticular sands in this area than longitudinal wave. This investigation also suggests that lenticular-type sand bodies might be delineated by the VSP method.

INTRODUCTION

A series of seismic investigations were performed at the Department of Energy Multi-Well Experiment (MWX) site, located approximately 9 miles west of Rifle, Garfield County, Co., on the southern bank of the Colorado River, in order to delineate the character of the lenticular-type sand beds within the Mesaverde Group in western Colorado and to determine the extent to which stimulation and production of gas can be achieved. To this end, a comprehensive seismic program was initiated to determine how well these discontinuous sand bodies could be mapped. This program was run in three separate phases: a high-resolution, three-dimensional survey; a vertical seismic profile; and a hole-to-hole survey (Searls and others, 1983).

This investigation focuses on the second phase of the program: the vertical seismic profiling method.

Three-component VSP data were recorded at the MWX 1 and MWX 2 wells from two surface-source locations. Analysis of far-offset VSP data at the MWX 2 well revealed that in addition to the longitudinal (P) wave, reliable shear waves--horizontally polarized shear (SH) and vertically polarized shear (SV) waves--were also recorded. Only vertical component data at the MWX 1 and MWX 2 wells from the near-offset source and three-component data at MWX 2 from the far-offset source were processed in detail and interpreted.

Processing of the near-offset VSP data was done by the methods described by Lee and Balch (1983), and processing of the three-component VSP data was done by the methods described in this report. Two processing techniques for processing far-offset, three-component VSP data are described in detail: one which solves problems associated with the random orientation of the horizontal component phones, and one which compensates for the effect of the source-offset distance.

Correlation between P-wave and SH-wave and correlation of seismic characters between wells were performed, and some acoustic parameters were estimated from the VSP data.

The main emphasis of this report is on the VSP data processing and to provide some pertinent information about the acoustic properties at the MWX well site. Detailed geological information at this area can be found in Lorentz (1983). The geological terms used in this report are from Lorentz (1983).

ACKNOWLEDGMENTS

Sincere appreciation is expressed to the CER Corporation, Sandia National Laboratory, U.S. Geological Survey, and the Department of Energy for their support of this investigation. I wish to thank A. H. Balch, J. J. Miller, L. W. Pankratz, and C. A. Searls for their field work, and Keith Westhusing, C. A. Searls, and C. W. Spencer for their stimulating discussions and encouragement.

FIELD PROCEDURE

VSP data were acquired during May of 1982 at the MWX well site located near Rifle, Colorado. The recording instrument was a 24-channel MDS 10, provided by the U.S. Geological Survey, and the surface seismic source was a Bolt 450 in.^{3} land airgun. Downhole geophones were tri-axial, three-component, and wall-locking, designed and provided by Sandia National Laboratory.

Two wells, MWX 1 and MWX 2, were available for the profiling. Each three-component downhole geophone was lowered into the MWX 1 and MWX 2 wells and recorded the seismic signal simultaneously. There were two different source locations used, with one near-offset (≈270 ft) and one far-offset (≈1,900 ft). The geometry of the well locations and source locations are shown in figure 1.

Data from each downhole phone were amplified in two stages with the output of each stage frequency modulating a constant bandwidth (4 kHz), voltage-controlled oscillator. The eight frequency modulated signals were frequency-division multiplexed and transmitted to the surface on a single-conductor wireline. The frequency-division multiplexed data were demodulated. The demodulated data were digitized and stored on digital magnetic tape. The record length was 3 seconds with 0.5 ms sampling interval, and 15 channels, shown in table 1, were recorded.

Most of the vertical component data recorded at the MWX 2 well with a high-gain set were useless because of the malfunctioning of the amplifier. Also, horizontal phones did not work properly for most of the recording time, so horizontal component data except that recorded at the MWX 2 well from the far-offset source were not considered for the detailed processing.

Near-offset VSP data were recorded from 8,000 ft to the surface with 25-ft depth sampling intervals, and 8,000 ft to 1,000 ft for the far-offset VSP data.

PROCESSING

Basic principles and procedures for the processing of near-offset VSP data were discussed in detail by Lee and Balch (1983). Because three-component, far-offset VSP data, in addition to near-offset data, were acquired at the MWX site, additional processing techniques were required and will be discussed in detail.

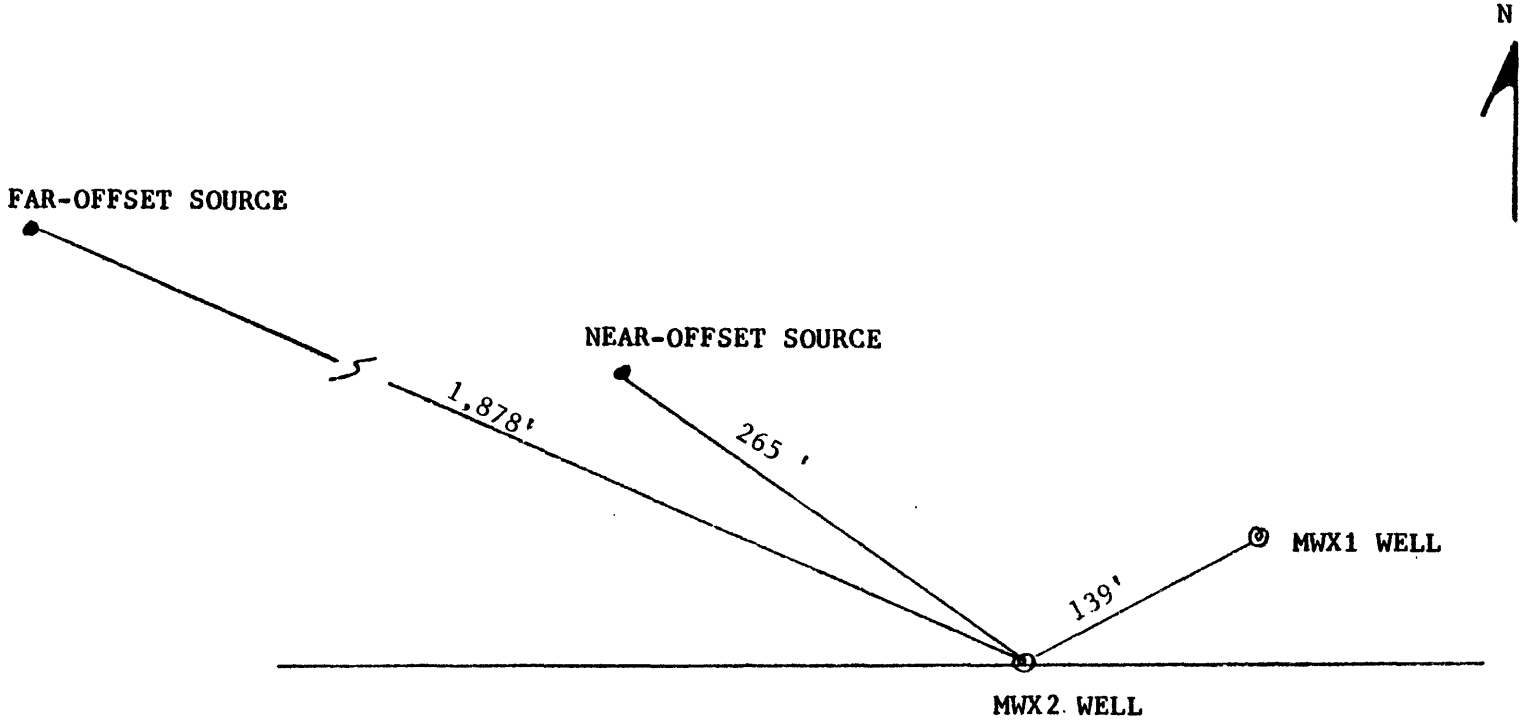

Figure 1.--VSP field layout at MWX well site near Rifle, Colorado.

Table 1.--Channel distribution of MDS 10 recording system for the VSP experiment at MWX well site, Garfield County, Co.

Channel No.	Component	Gain	Well	Comments
1	vertical	high	MWX 1	Horizontal component phones did not work properly.
2	horizontal 1			
3	horizontal 2			
4	vertical	low		
5	horizontal 1			
6	horizontal 2			
7	vertical	high	MWX 2	Horizontal component phones, except for the far-offset source, and high gain set did not work properly.
8	horizontal 1			
9	horizontal 2			
10	vertical	low		
11	horizontal 1			
12	horizontal 2			
13	monitor	100 ft below the source		
14	time break			
15	uphole	near the source		

Near-Offset VSP Data

The general processing sequence used for the near-offset VSP data is shown in figure 2. Only brief discussions of some important processing sequences applied to these data are included.

The raw field data were plotted and edited for bad traces. Figure 3 shows an example of the raw vertical component data at the downhole-geophone locations from 6,000 ft to 5,875 ft. Those traces which did not have consistent time breaks, were excessively noisy, or that did not otherwise conform to the other data recorded at the same geophone location were eliminated from further processing. The only good traces, recorded at the same geophone location, were summed to improve signal-to-noise ratio.

Ideally, one would energize the seismic source only once and record at all depth levels simultaneously. However, only one depth level at a time can be recorded due to instrument constraint. In all VSP processing techniques, source waveforms are assumed to be identical at each depth level. However, this assumption is not always valid. Figure 4 shows the monitor-phone record and amplitude spectrum when the downhole geophone was at 7,025 ft and figure 5 shows the monitor-phone record when the downhole geophone was at 2,275 ft. Notice a substantial change of the source waveform. Utilizing the information contained in the monitor phone, the source waveform changes can be compensated.

Figure 6 shows the vertical component VSP data at the MWX 2 well which were processed up to gain application. From this figure, strong downgoing-body waves, weak upgoing-reflected waves, and tube waves can be observed.

The most important processing step in understanding and interpreting VSP data is to separate upgoing waves from downgoing waves. At the same time, the coherent noise, such as tube waves, should be suppressed. This decomposition of the wave field can be accomplished by using multichannel, velocity filtering. In this report, all the velocity filterings were done in the frequency-wavenumber (F-K) domain. Figure 7 shows the desired downgoing wave fields from data shown in figure 6, and figure 8 shows the separated upgoing waves.

The downgoing waves from the source is neither an impulse nor a simple wavelet, but a complicated wave train. Reverberation of seismic energy trapped in the near surface is largely responsible for this phenomenom. The downgoing waves shown in figure 7 have substantial amplitude up to 400 ms from the onset time. In this circumstance, the geologic interpretation can be difficult. It is necessary to compute the data set that would have been recorded if the original downward-traveling wave train had been a single short pulse. This is the essence of downgoing wave-train deconvolution.

Figure 9a shows the downgoing waves and amplitude spectra at 3,025 ft before deconvolution, and figure 9b shows the result of downgoing wave-train deconvolution. The improvement is quite substantial.

Cumulative summation is a powerful signal-to-noise enhancement processing technique.

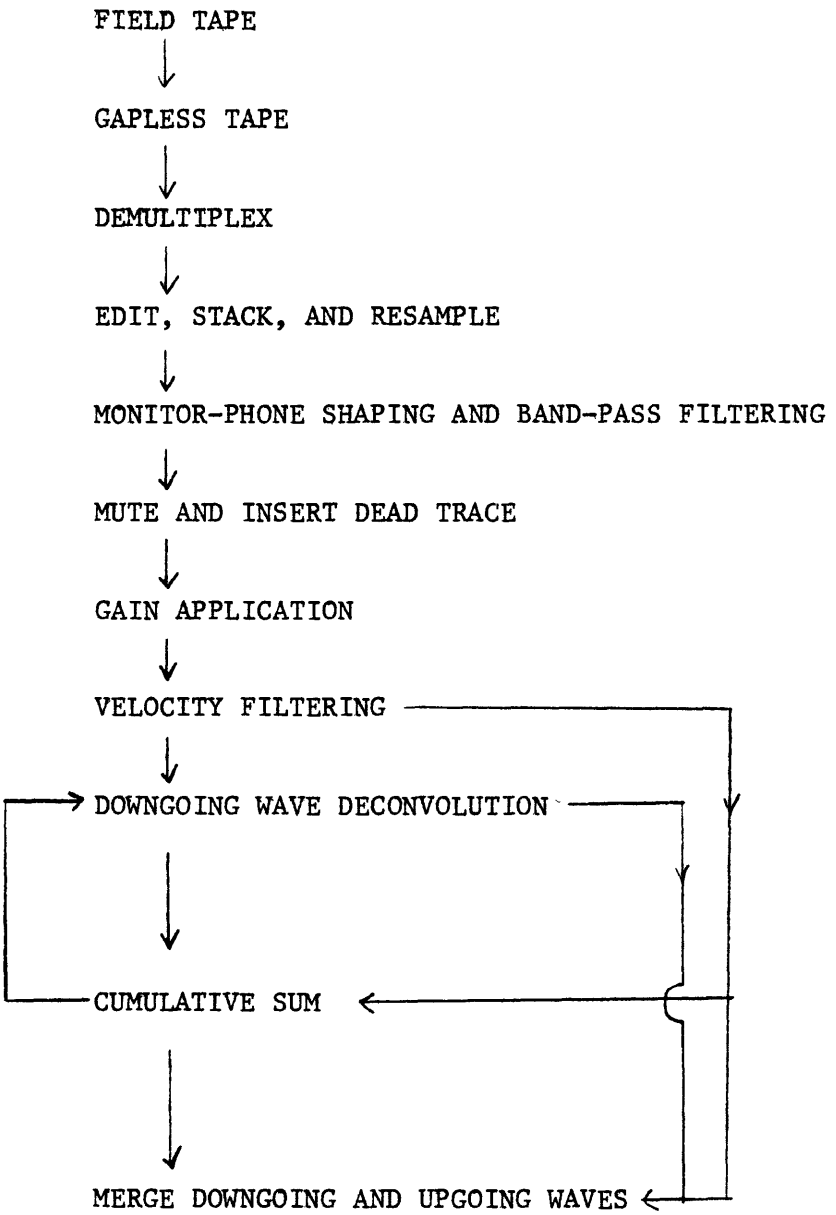

Figure 2.--General processing flow sheet for the vertical-component, near-offset VSP data.

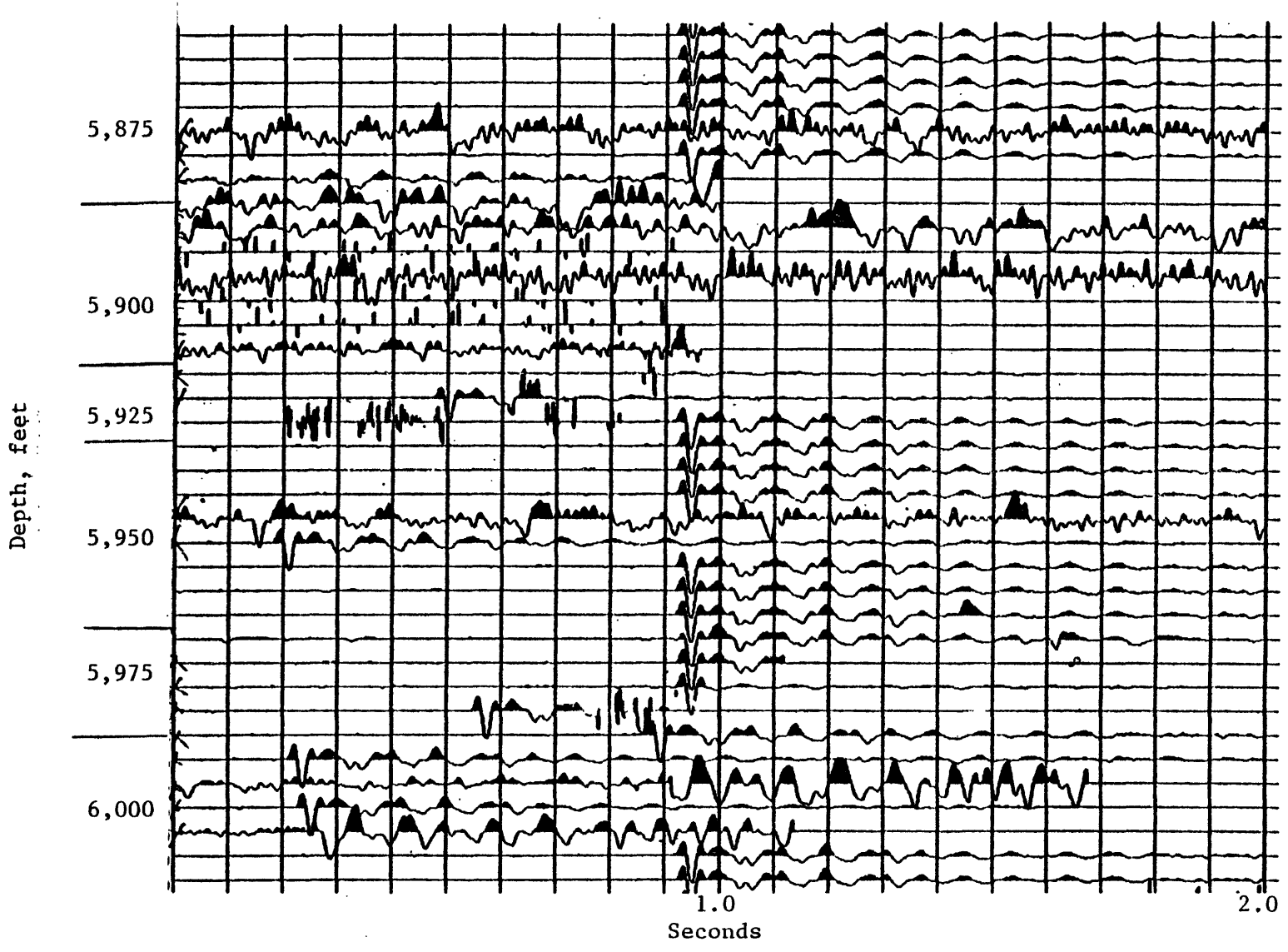

Figure 3.--Raw VSP data at MWX 2 well from the near-offset source.

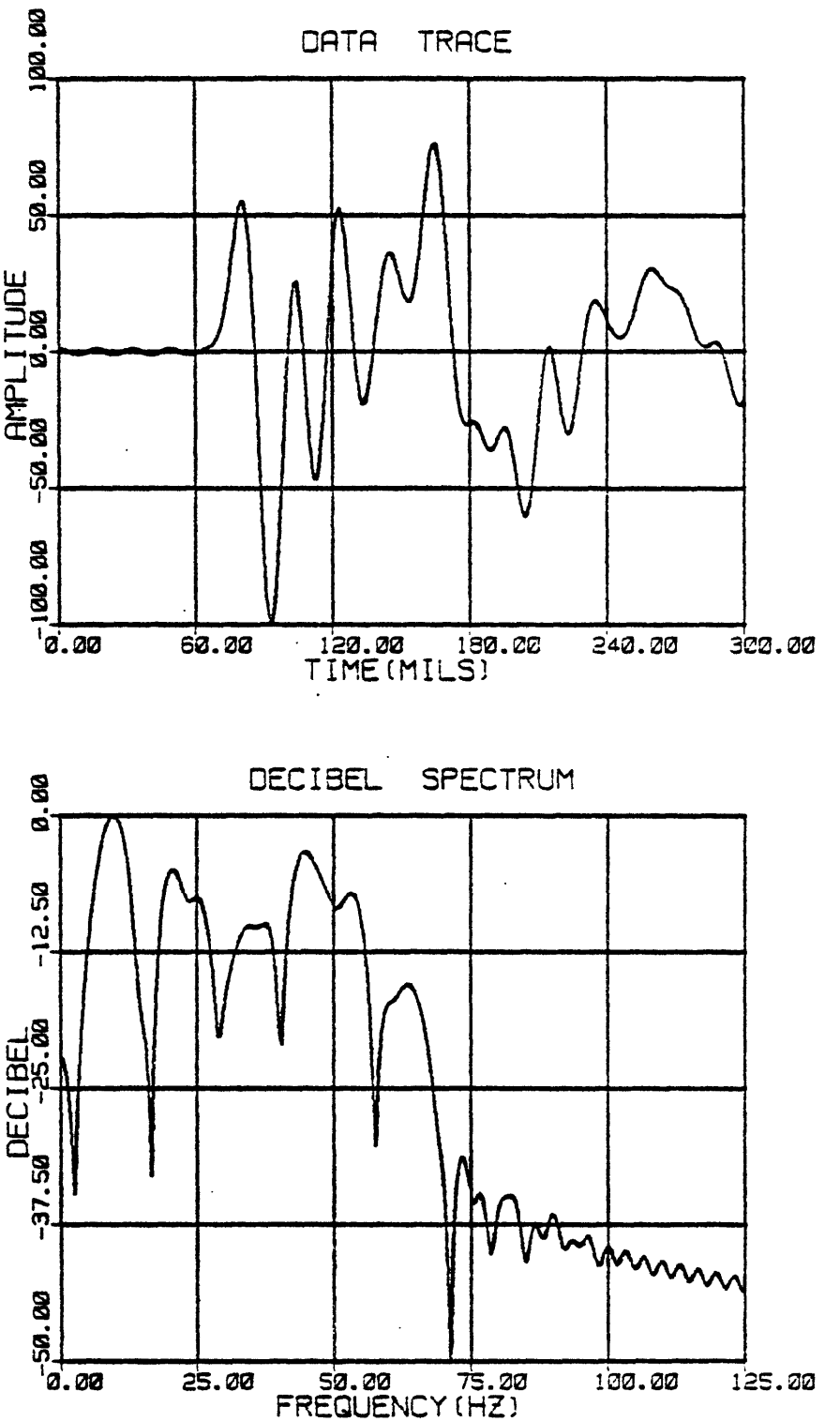

Figure 4.--Monitor-phone record (top) and its amplitude spectrum (bottom) at the well-phone depth level of 7,025 ft.

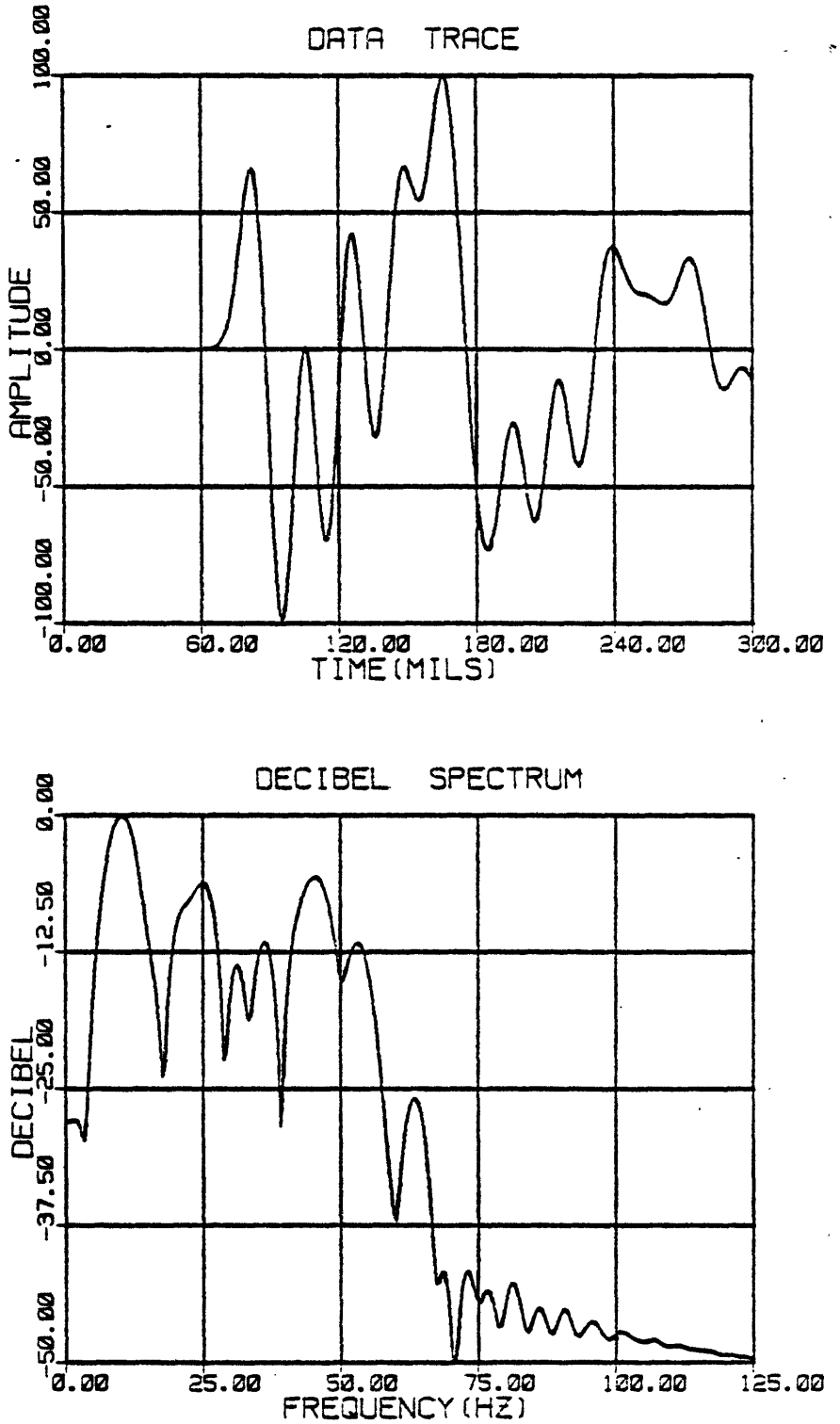

Figure 5.--Monitor-phone record (top) and its amplitude spectrum (bottom) at the well-phone depth level of 3,025 ft.

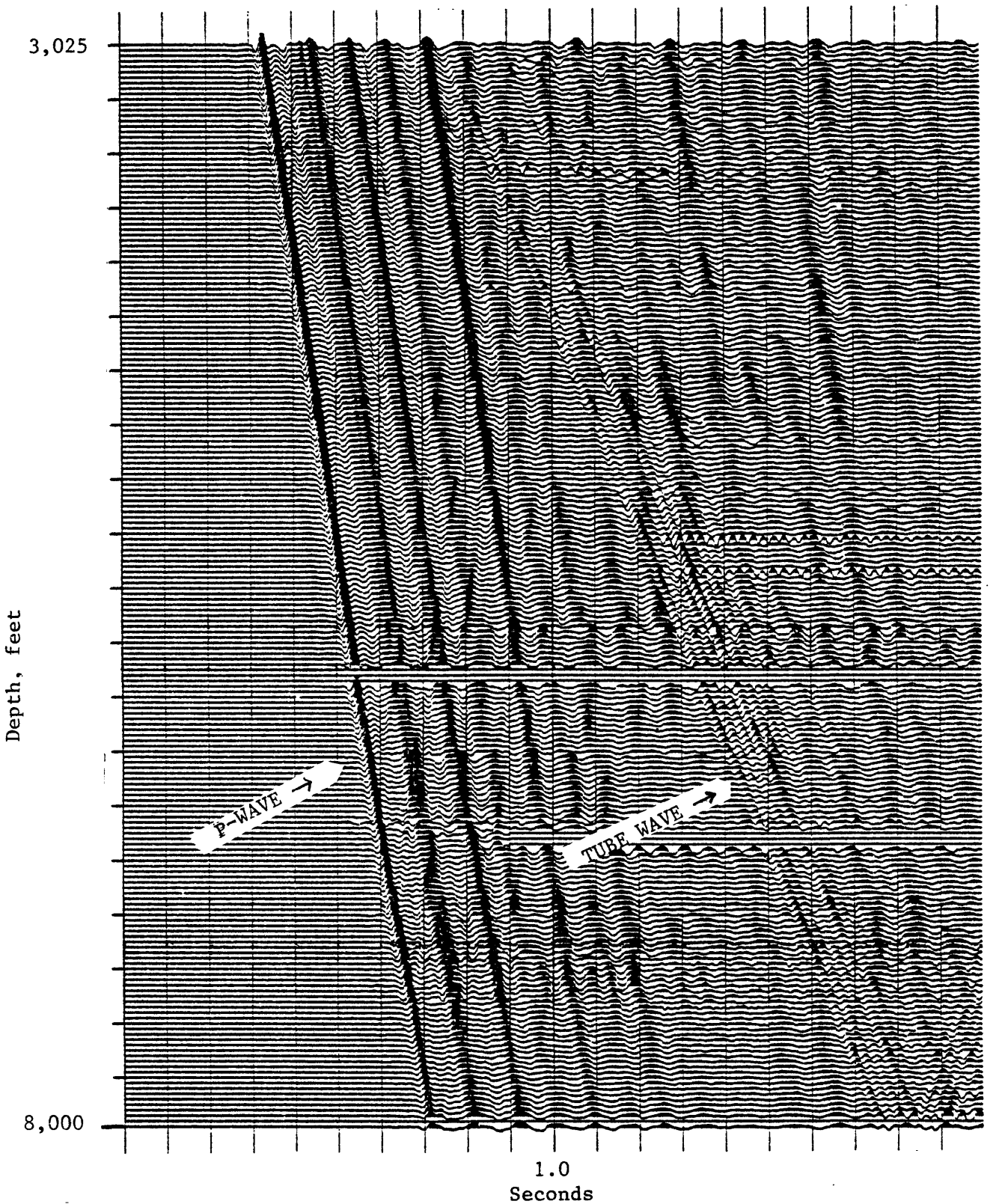

Figure 6.--Near-offset vertical component VSP data at MWX 2 well with 25-ft trace interval.

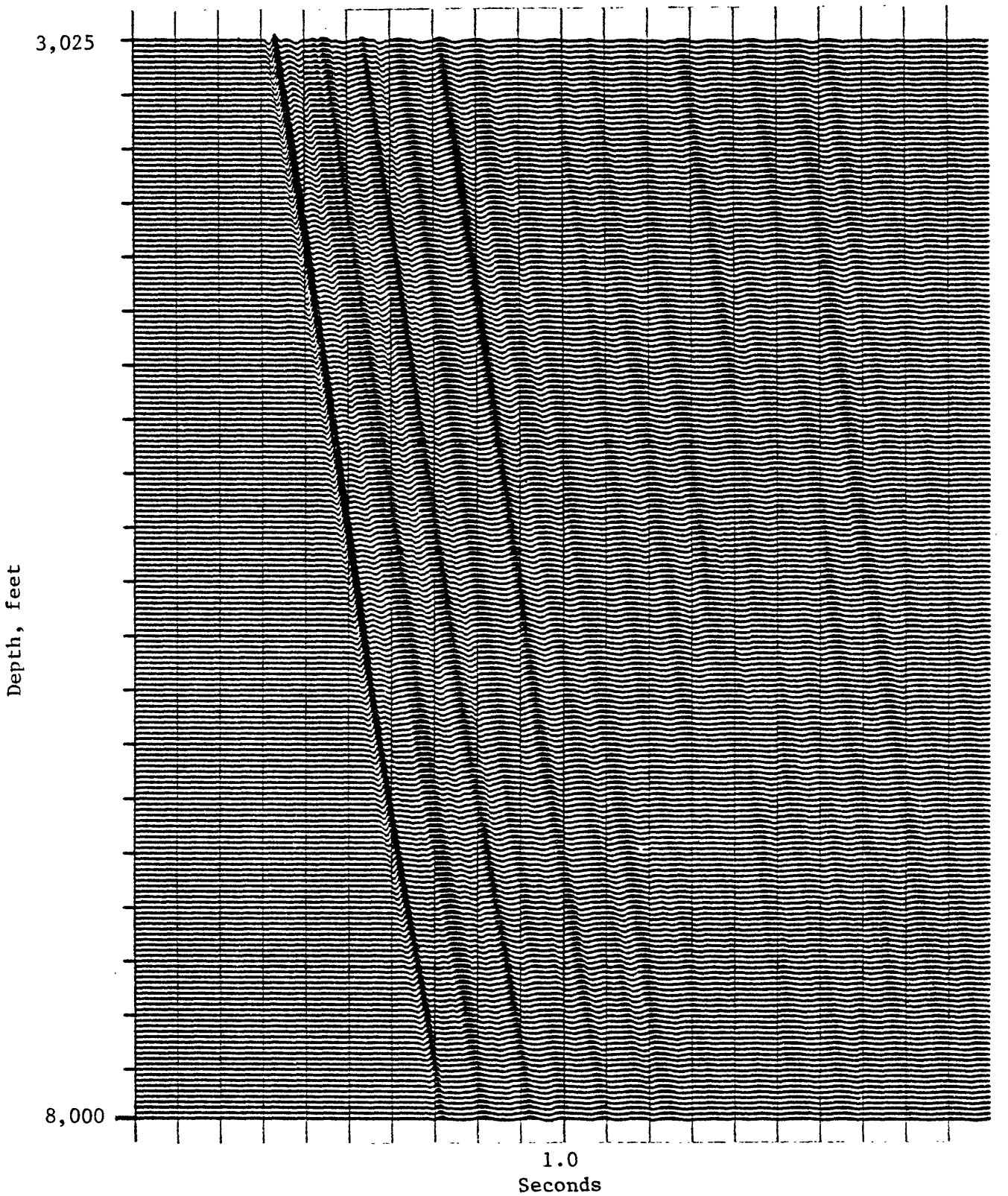

Figure 7.--Downgoing waves of figure 6.

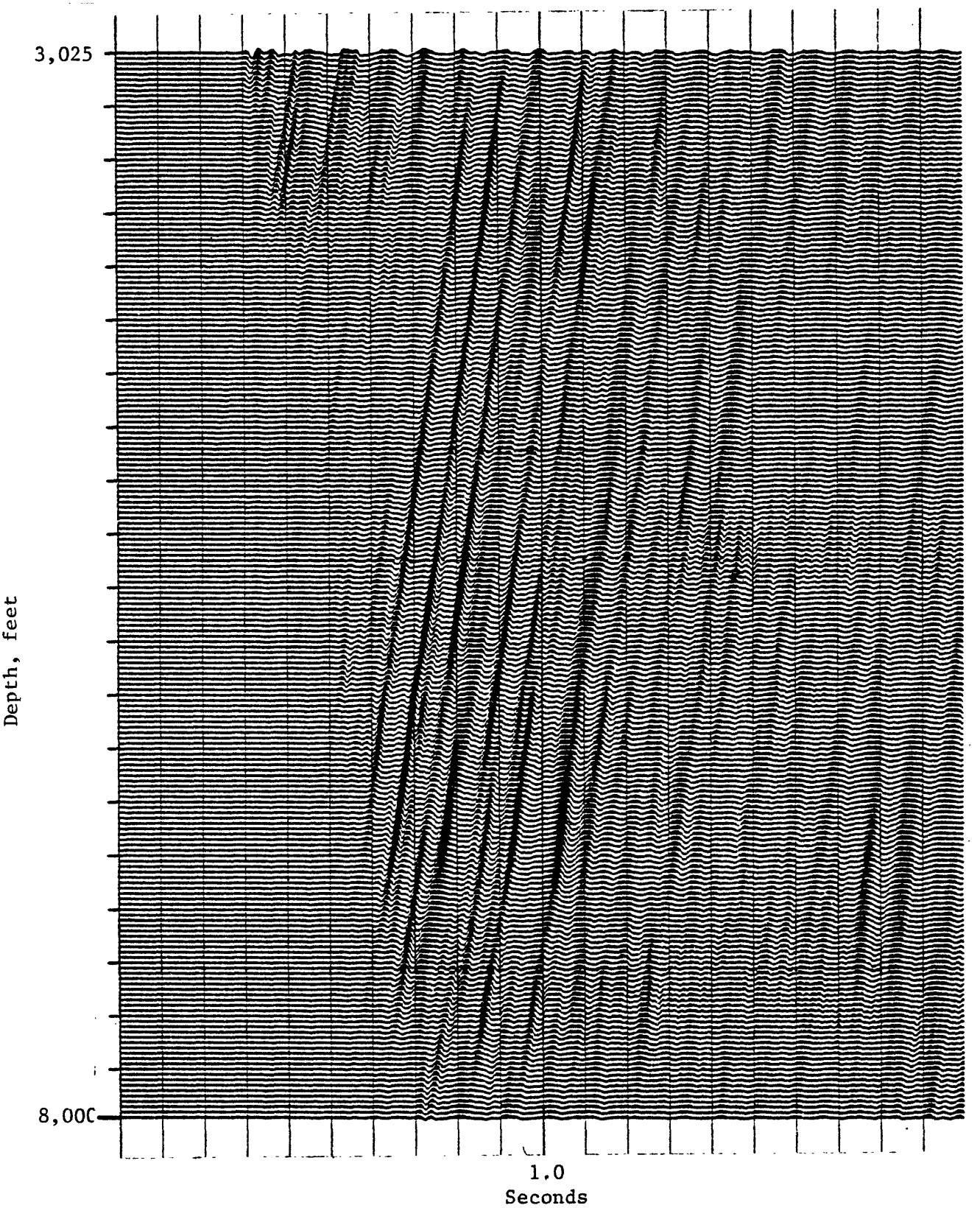

Figure 8.--Upgoing waves of figure 6.

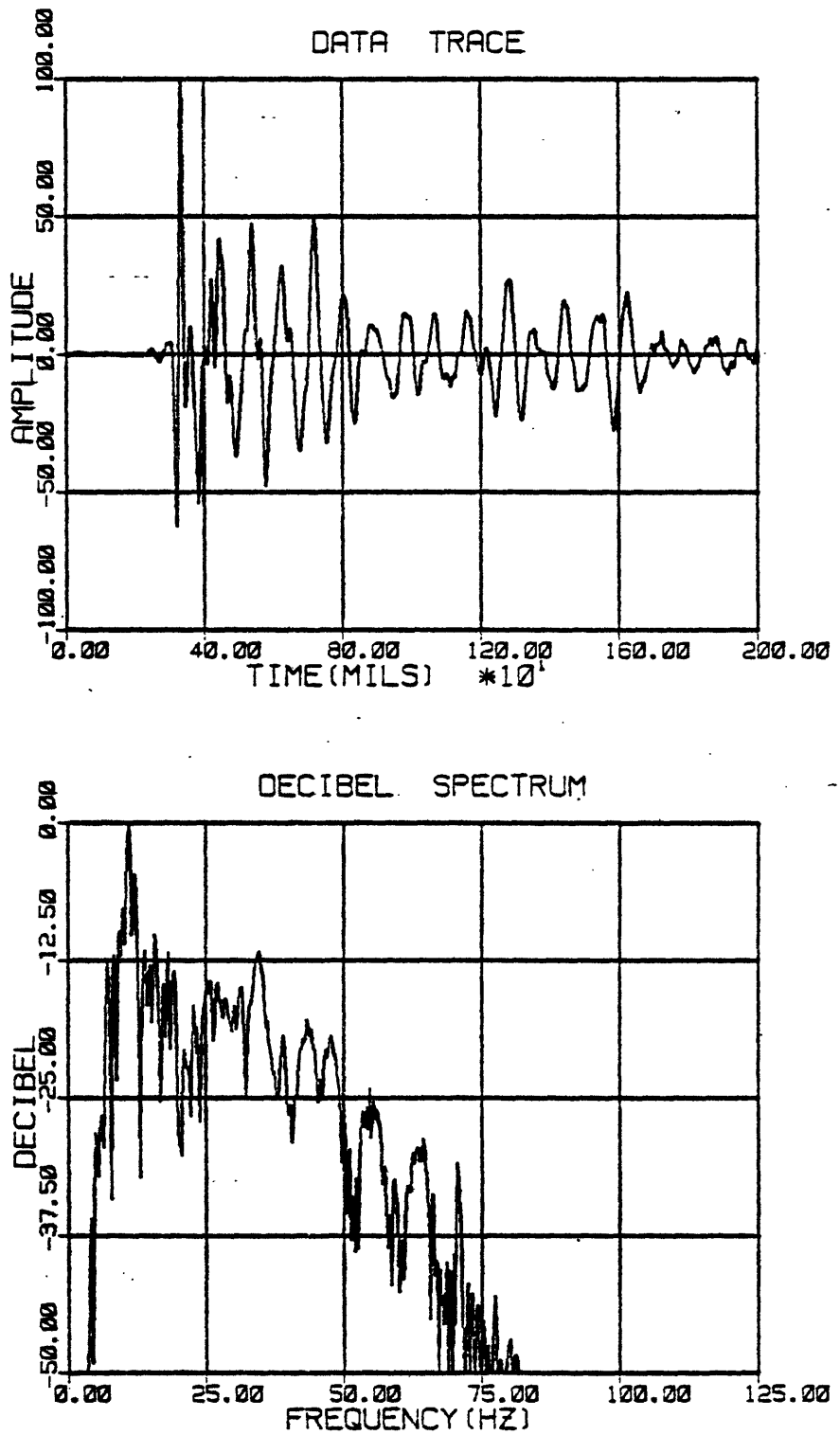

Figure 9a.--Downgoing wave at the depth level of 3,025 ft (top) and its amplitude spectrum (bottom).

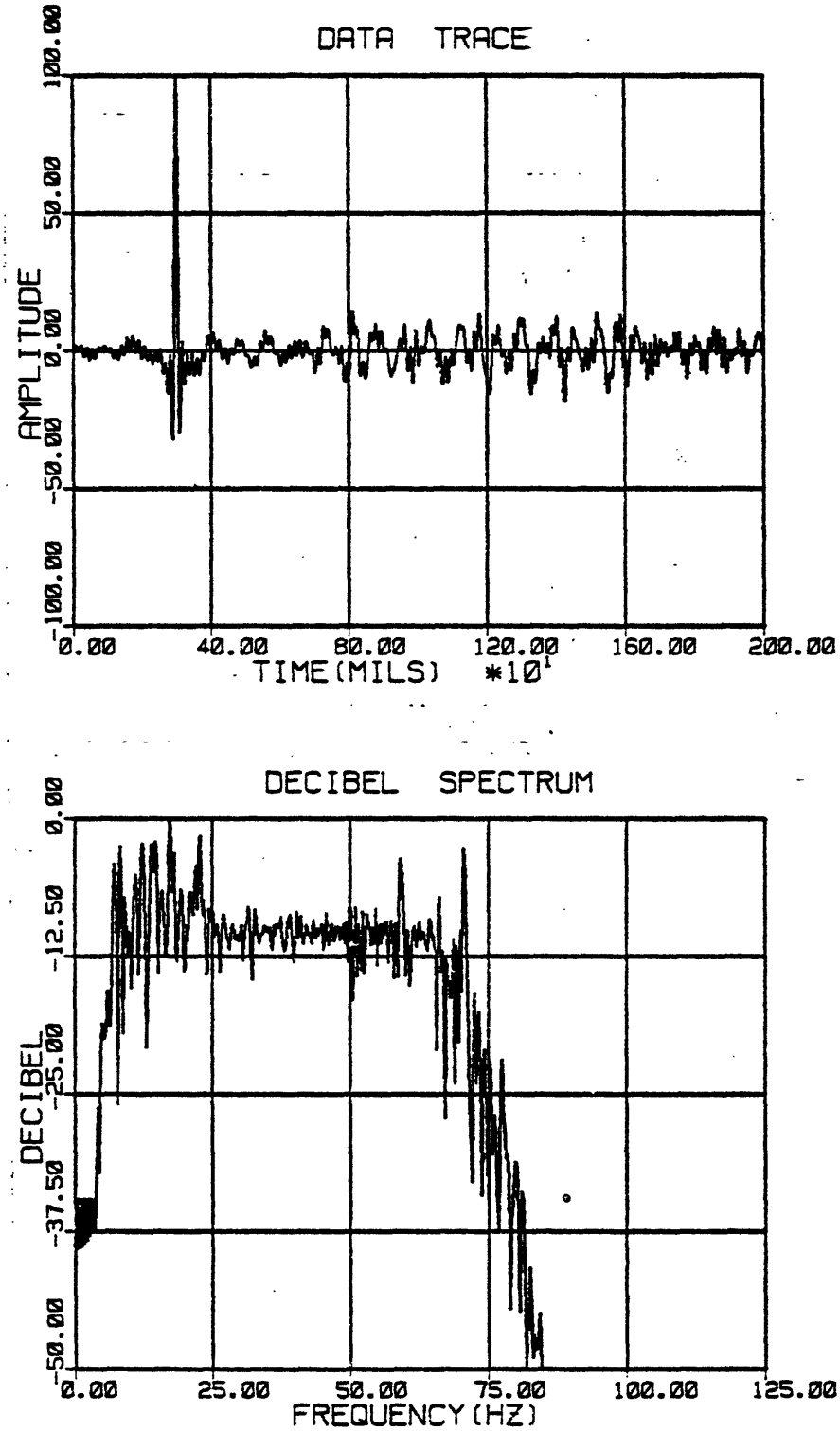

Figure 9b.--Downgoing wave at the depth level of 3,025 ft (top) and its amplitude spectrum (bottom) after downgoing wave deconvolution.

Cumulative summation is defined by the following formula:

$$\bar{S}_J(t) = \sum_{i=1}^{J} S_i(t-\Delta t_i)A_J(t)$$

where

$\bar{S}_J(t)$: cumulative summed trace at depth level J,

$S_i(t)$: input trace at depth level i,

Δt_i: time shift amount at depth level i in order to align the upgoing waves vertically, and

$A_J(t)$: amplitude compensation function.

The cumulative summation fails to show the detailed changes in waveforms and amplitudes as the upgoing reflected events move upward. On the other hand, very small amplitude reflections, deep in the ground, are enormously enhanced, so this processing technique is very effective in tying surface reflection data with VSP data.

Figure 10 shows cumulative summed upgoing waves at the MWX 2 well, with application of the downgoing wave train deconvolution. Downgoing wave deconvolution operator was designed at the depth level of 3,025 ft, and the same operator was applied to the whole section shown in figure 8.

Far-Offset VSP Data

Most of the processing sequences for far-offset VSP data are very similar to those of near-offset VSP data. All of the steps shown in figure 2 can be applied to the far-offset VSP data processing. However, due to the difference of source-receiver geometry, some of the processing steps should be modified and additional techniques should be developed.

Generally, far-offset VSP data are more complicated than near-offset VSP data mainly because of the presence of shear waves, converted waves, and critically reflected waves in addition to the transmitted and reflected longitudinal waves. Kinematics and dynamics of the wave field are important in analyzing all the different modes of propagation. Therefore, it is essential to have three-component VSP data for the analysis of the far-offset data.

To utilize three-component data, the orientation of the horizontal components of the downhole geophones to some fixed reference frame should be known. Presently, the measuring of the relative orientation of the downhole geophone is not available. Thus, in order to process the three-component data, the random orientations between depths should be removed by orienting the observed data to a fixed reference frame.

Once the ambiguities of the orientation of the horizontal component data are resolved, multichannel filtering may be applied to enhance selected modes of propagation, and downgoing wave-train deconvolution may be used in order to increase vertical resolution. Also, vertical stacking may be applied to enhance signal-to-noise ratio. To implement the stacking procedure effectively, a method of compensating for source-offset distance is needed.

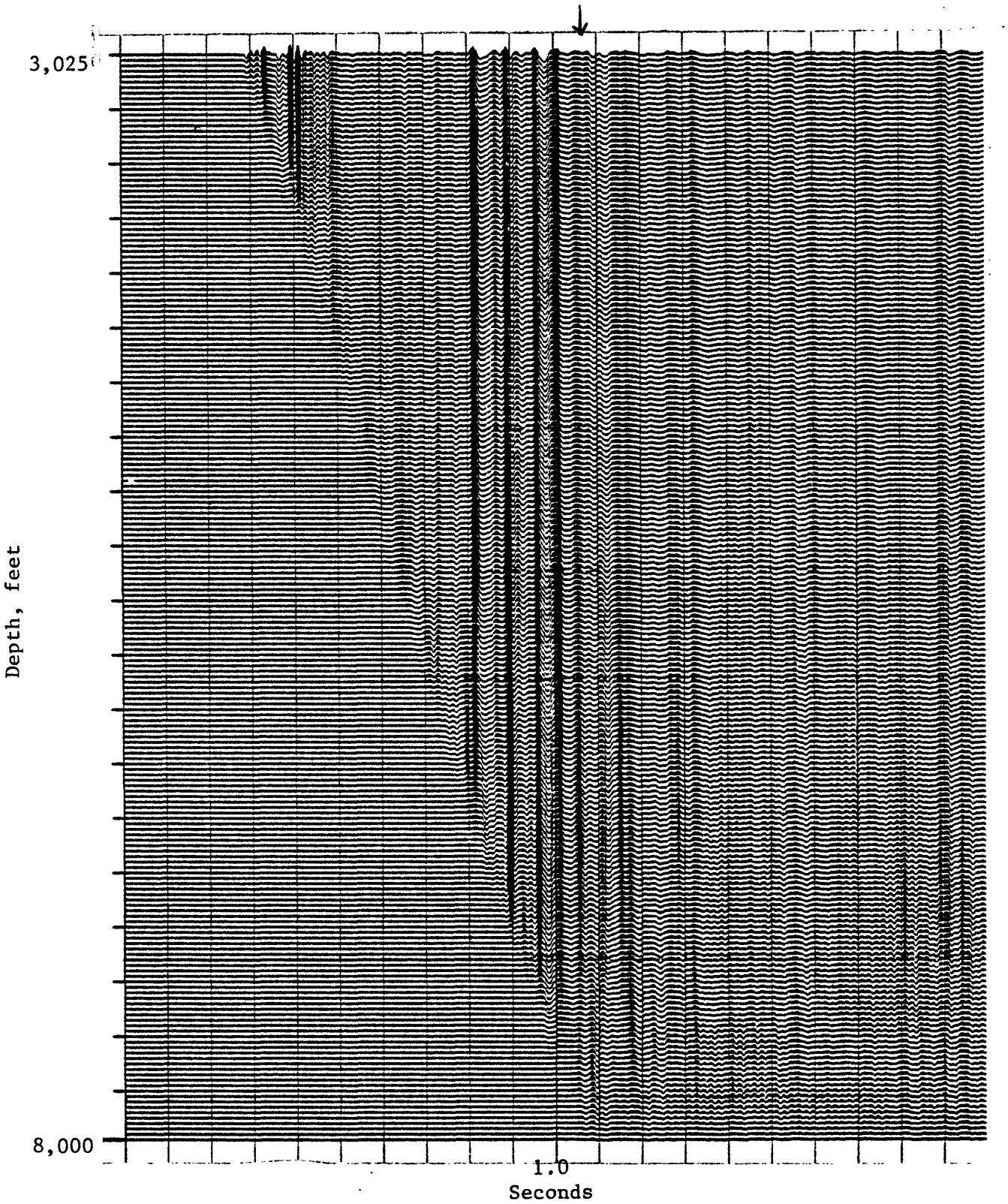

Figure 10.--Cumulative-summed, vertical-component upgoing waves at MWX 2, processed from the data shown in figure 6.

Additional steps considered in order to process the three-component far-offset VSP data at the MWX well are: 1) orientation of the horizontal component data, and 2) dynamic time correction. In the following sections, each additional processing step is discussed in detail. The processing sequence used to process far-offset VSP data at the MWX well site is shown in figure 11.

Orientation of the horizontal phones.--Define orthogonal Cartesian coordinate system (X, Y, Z) in such a way that Z-axis is along the vertical borehole, X-axis is in the direction of the source location, and Y-axis is the perpendicular direction of X-Z plane.

This coordinate system is a fixed reference frame. Let (X_o, Y_o, Z_o) be the local orthogonal Cartesian coordinate system fixed at one particular depth point, where Z_o-axis is the same as Z-axis. The three-component geophone can twist and rotate randomly from depth to depth during the recording period. Therefore this local coordinate system (X_o, Y_o, Z_o) is a random function of a recording depth with respect to a fixed reference frame (X, Y, Z).

The orientation of the horizontal component data can be accomplished by coordinate transformation between the reference coordinate system and the local coordinate system under the assumption that longitudinal wave motion is linearly polarized.

Figure 12 schematically illustrates the raypath of P-wave from the source to the downhole geophone for an isotropic and homogeneous media. The particle motion of the P-wave is assumed to be along the raypath. In the reference coordinate system, the particle motion of P-wave along the raypath can be decomposed into vertical component V_Z and horizontal component V_X. There is no horizontal component V_Y due to the linear polarization assumption.

The relative orientation of the observed horizontal component V_{X_o} and V_{Y_o} with respect to the reference frame is also shown in Figure 12. Let Θ be the angle between X- and X_o-axis. Then using coordinate transformation, the following equation can be derived:

$$V_X = V_{X_o} \cos\Theta - V_{Y_o} \sin\Theta$$
$$V_Y = V_{X_o} \sin\Theta + V_{Y_o} \cos\Theta. \qquad (1)$$

If Θ can be estimated from the observed data, the observed data can be decomposed into the reference coordinate system using Equation (1).

As mentioned previously, the P-wave has only the V_X horizontal component. Therefore, one way to estimate Θ is to find an angle where the energy of V_X component data is maximized.

The quantity which is proportional to energy is defined as

$$E(\Theta) = \int_{T_1}^{T_2} V_x^2(t)dt = \int_{T_1}^{T_2} \left[V_{x_o}(t)\cos\Theta - V_{y_o}(t)\sin\Theta\right]^2 dt$$

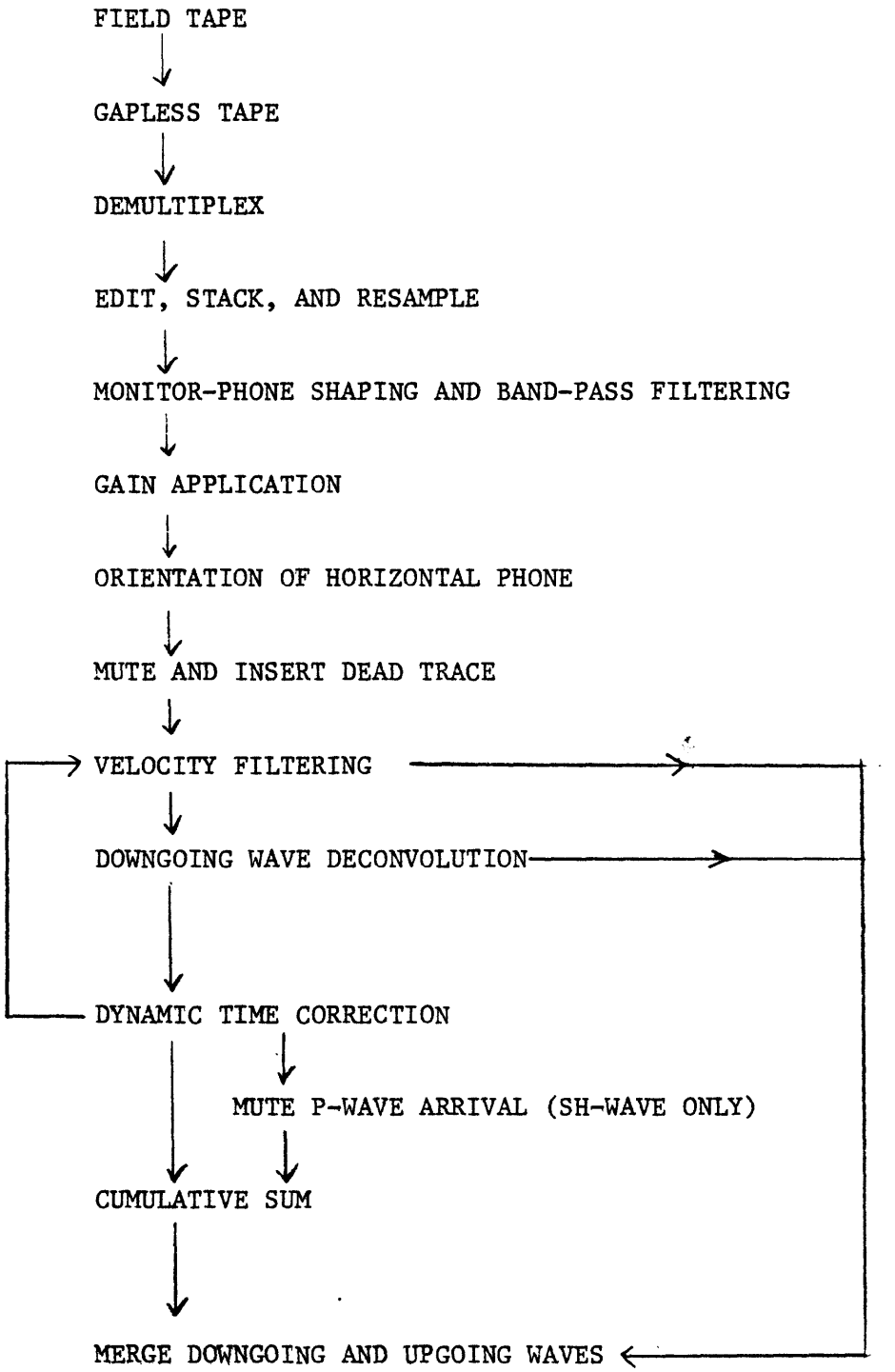

Figure 11.--General processing flow sheet for the three-component, far-offset VSP data at MWX 2 well.

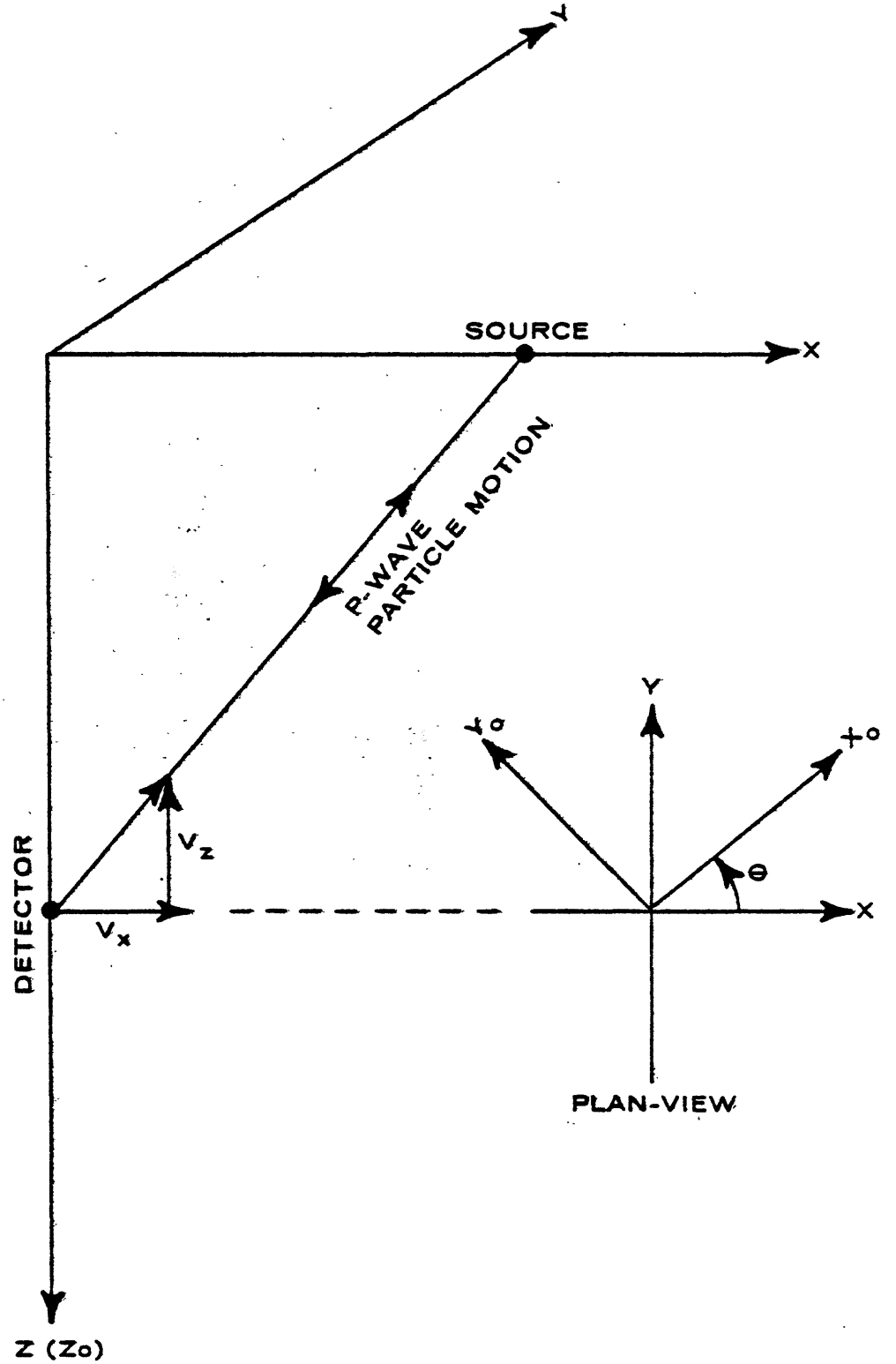

Figure 12.--Diagram showing particle motion, reference coordinate system (X, Y, Z), and local coordinate system (X_o, Y_o, Z_o) for the orientation of horizontal components of data.

where T_1 and T_2 is a window for the P-wave arrival. Maximizing $E(\theta)$, it can be shown that

$$\theta_{max} = \frac{1}{2} \tan^{-1} \left[\frac{2\int_{T_1}^{T_2} V_{x_o} V_{y_o} dt}{\int_{T_1}^{T_2} (V_{y_o}^2 - V_{x_o}^2) dt} \right] \qquad (2)$$

Notice that when $V_{Y_o} = 0$, $\theta_{max} = 0$ or 180^o. This means that the local coordinate system (X_o, Y_o) is identical to the reference coordinate system.

When $\theta = \theta_{max} + 180^o$, there is no difference between the energy. Therefore, the polarities of the vertical component data may be used to resolve the ambiguity of the horizontal component polarities.

Figure 13a shows an example of the unoriented horizontal component data, acquired at the MWX 2 well. The observed horizontal component data shows abrupt changes of amplitudes and arrival times, mainly because of the random orientation of the three-component well phone.

The results of applying the orientation technique is shown in Figure 13b. The improvement of data quality is substantial. The X-component data (in-line) shows the consistant arrival times and amplitude variation, and the amplitudes of Y-component (transverse) of the first arrivals of P-wave are very small as predicted.

Dynamic time correction.--In near-offset VSP sections, the magnitude of moveout times of upgoing waves from the horizontally layered media are the same as the downgoing wave moveout time. Therefore, it is simple to vertically align the upgoing waves and apply vertical stacking in order to enhance the signal-to-noise ratio. When the source offset distance is not negligible compared with the reflecting horizon, the downgoing moveout is quite different from the upgoing waves.

In conventional surface seismograms, the shot offset correction (NMO correction) is very well understood and simple for horizontally layered media. In the VSP, the dynamic-time correction (source-offset correction) is more complicated, mainly because the downgoing path of the reflected event is different from the upgoing path.

The raypath geometry used in the dynamic time correction is illustrated in Figure 14, where

- l: shot offset distance,
- H: a reflector depth,
- Z: well-geophone location, and
- V: medium velocity.

The reflected arrival time is given by

$$T_1 = \frac{\sqrt{l^2 + (2H-Z)^2}}{V} = T_o \sqrt{1 + \frac{l^2}{T_o^2 V^2}}$$

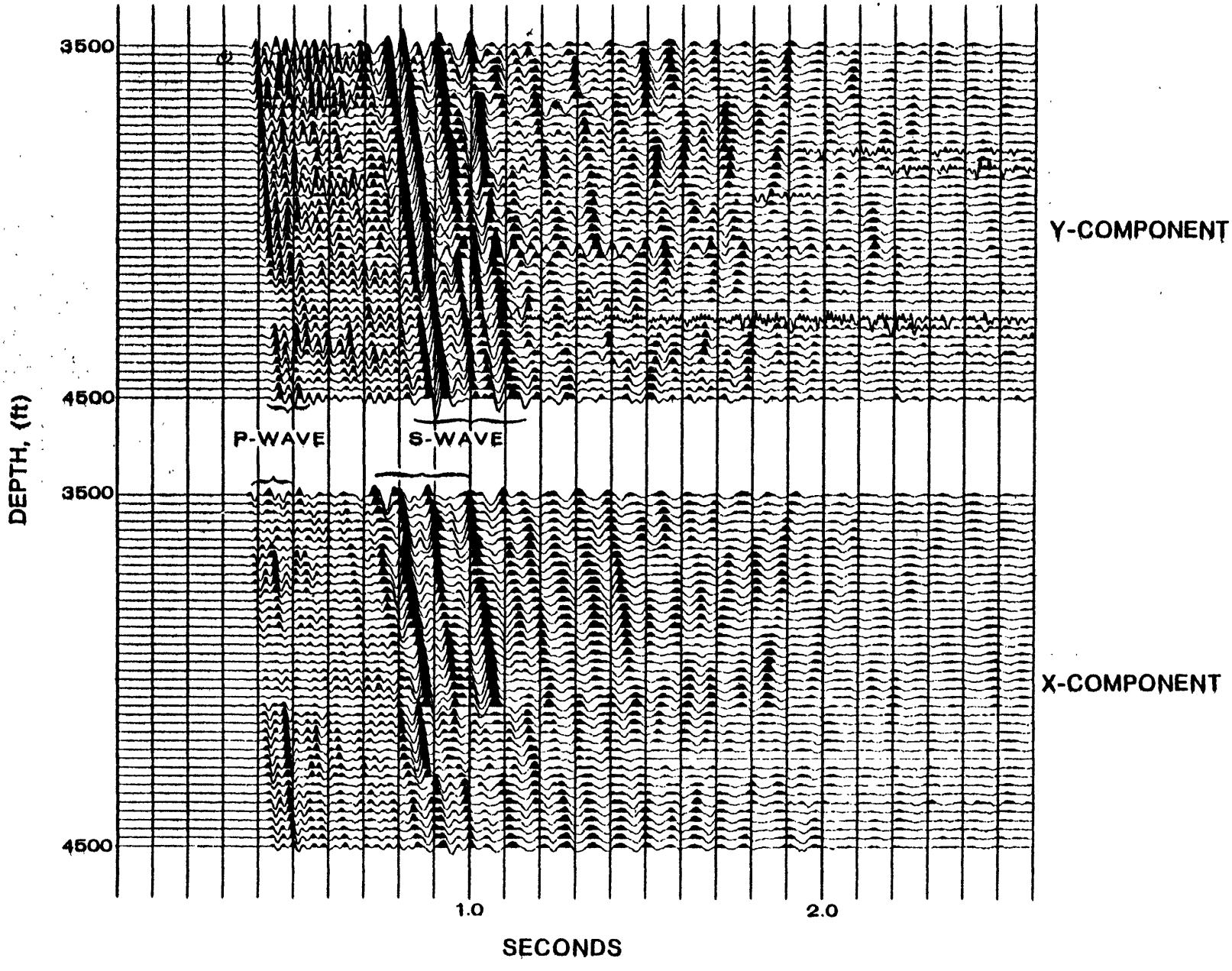

Figure 13a.--Example showing the effect of orientation of horizontal-component VSP data at MWX 2 well. Original horizontal-component data.

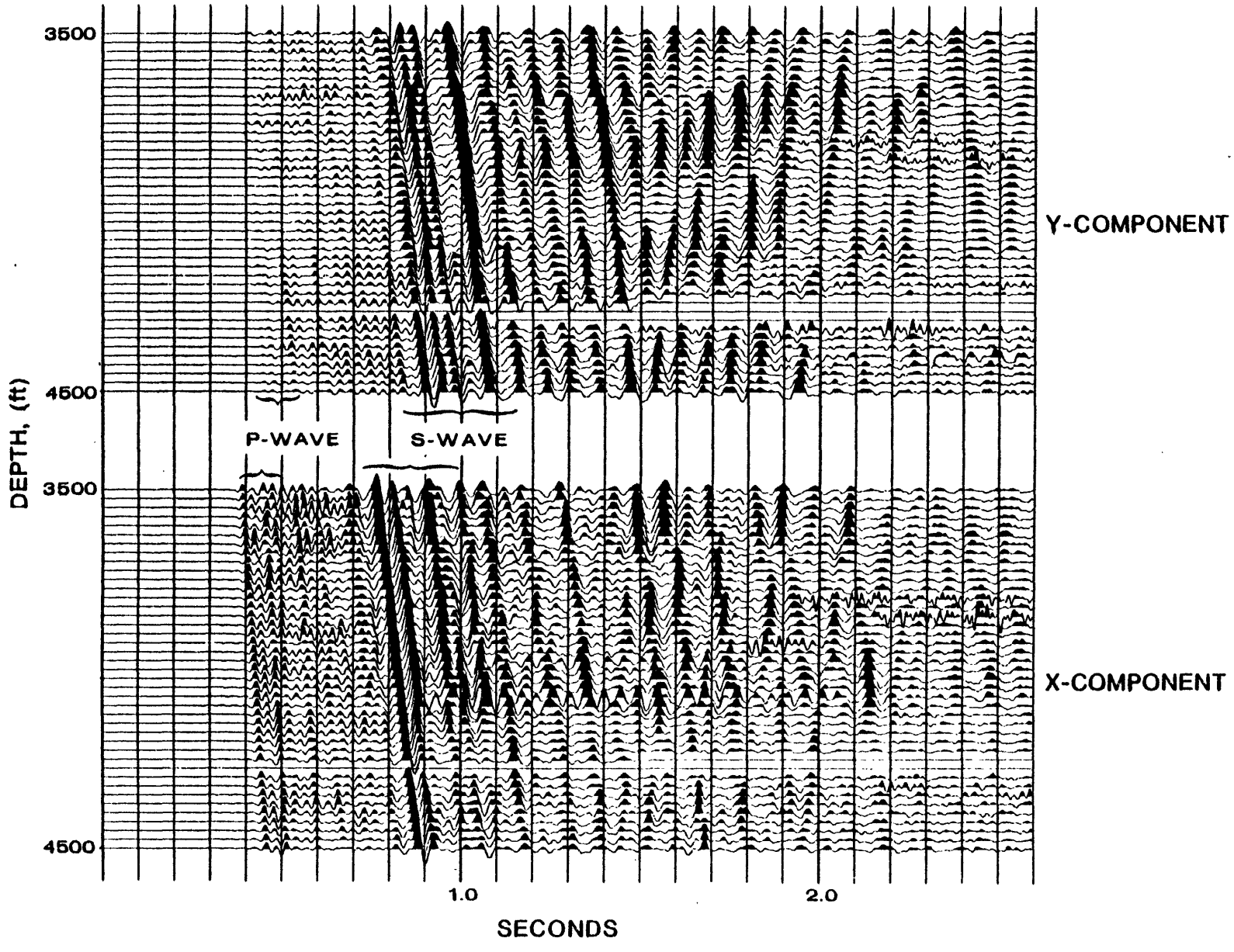

Figure 13b.--Example showing the effect of orientation of horizontal-component data at MWX 2 well. Oriented horizontal-component data.

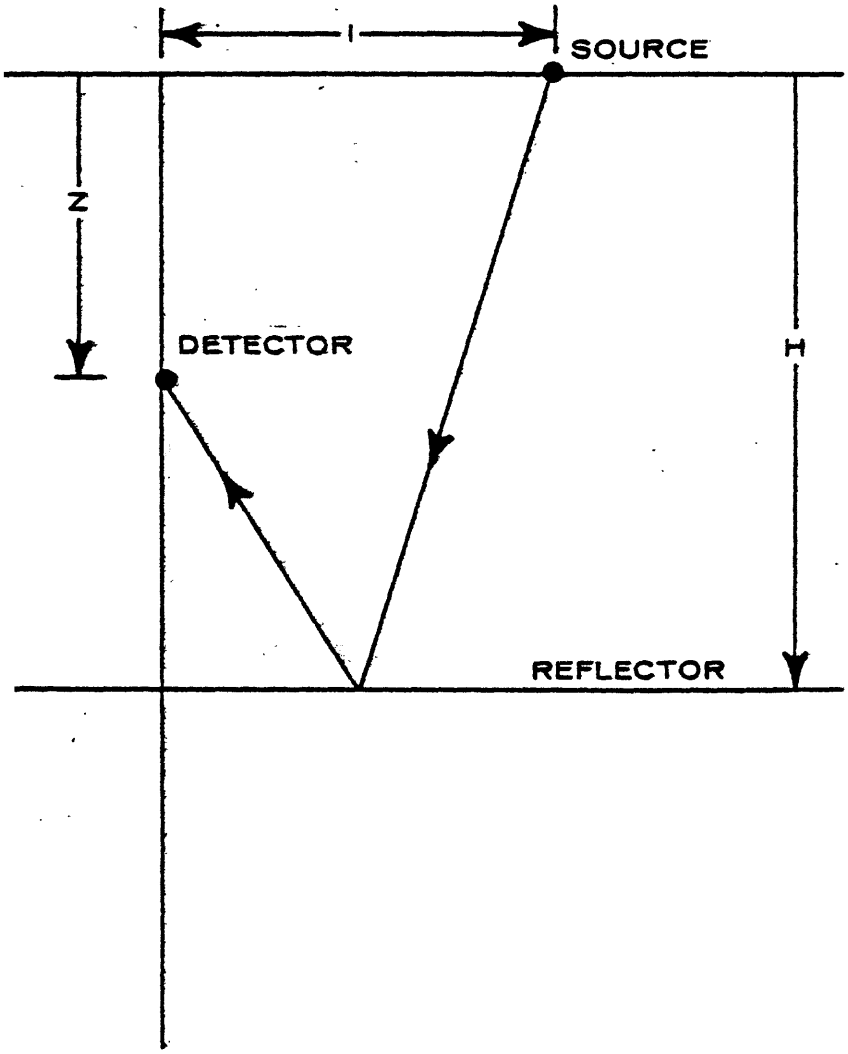

Figure 14.--Schematic raypath diagram for a dynamic time correction.

where T_o is the zero offset (l = 0) reflected arrival time. The dynamic time correction is defined by

$$\Delta T = T_l - T_o = T_o \left[\sqrt{1 + \frac{l^2}{T_o^2 V^2}} - 1 \right] \tag{3}$$

In the homogeneous medium, the dynamic time correction is very simple. Since T_o is a function of geophone location Z, the dynamic correction for the upgoing waves are depth dependent.

In the heterogeneous media, the dynamic time correction may be written as:

$$\Delta T_{z,n} = T_{o,n} \left[\sqrt{1 + \frac{l^2}{T_{o,n}^2 V_{NMO}^2}} - 1 \right] \tag{4}$$

where $\Delta T_{Z,n}$ is the dynamic time correction applied at the well-geophone location Z for the reflection from the n-th interface, $T_{o,n}$ is the corresponding zero-offset travel time, and V_{NMO} is the velocity to be used for the dynamic time correction.

If the source offset distance is not large compared to the depth of the reflector, V_{NMO} in Equation (4) can be substituted by $V_{NMO} \cong V_{RMS}(T_R)$, from Brown (1969), where $V_{RMS}(T_R)$ is the root mean square (RMS) velocity along the reflection path.

Therefore, the equation for the dynamic time correction for far-offset VSP data is the same as the normal moveout correction for a conventional surface seismic profile. To apply Equation (4) to the VSP data, V_{RMS} must be estimated as a function of geophone location Z along the reflection path.

Assume that a well geophone is located in the j-th interface (see Figure 15), and a reflector is located in the n-th interface. Then the RMS velocity along the reflection path, $V_{RMS}(T_R)$, can be written

$$V_{RMS}(T_R) = \frac{2 \sum_{i=1}^{n} V_i^2 t_i - \sum_{i=1}^{J} V_i^2 t_i}{2 \sum_{i=1}^{n} t_i - \sum_{i=1}^{J} t_i} \tag{5}$$

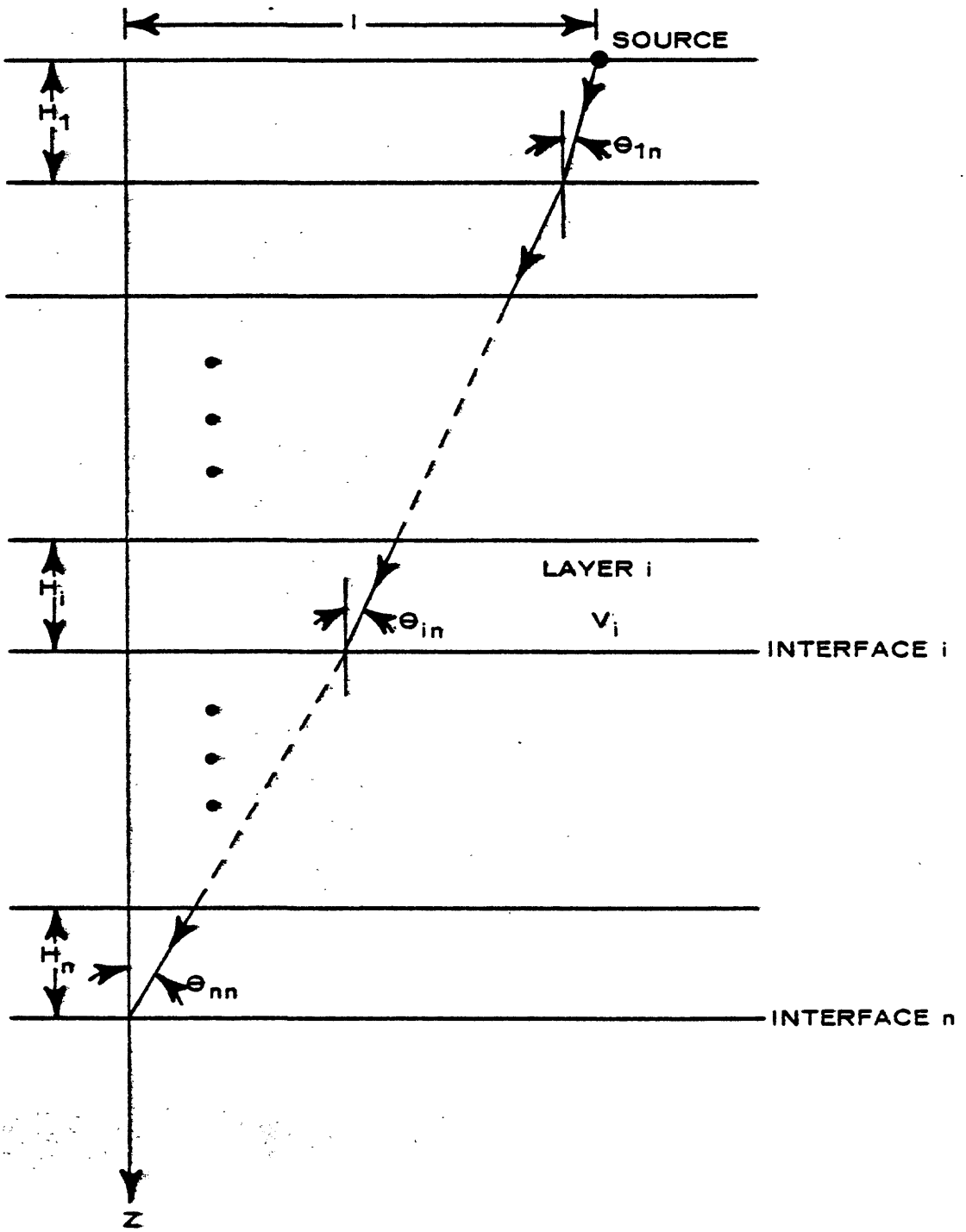

Figure 15.--Schematic raypath diagram for a multi-layered media.

where t_i and V_i are the one-way vertical travel time and medium velocity in the i-th layer, respectively.

Equation (5) can be rewritten as:

$$V_{RMS}(T_R) = V_{RMS}(T_n) + \frac{[V_{RMS}(T_n) - V_{RMS}(T_z)]Z}{T_{o,n}\,\overline{V}(Z)} \tag{6}$$

where

$$T_n = \sum_{i=1}^{n} t_i$$

$$T_Z = T_J = \sum_{i=1}^{J} t_i$$

$$\overline{V}_{(Z)} = \frac{Z}{T_Z} = \frac{\sum_{i=1}^{J} V_i t^i}{T_J}$$

$$V_{RMS}(T_n) = \frac{\sum_{i=1}^{n} V_i^2 t_i}{T_n}$$

$$V_{RMS}(T_Z) = V_{RMS}(T_J) = \frac{\sum_{i=1}^{J} V_i^2 t_i}{T_J}$$

and $$T_{o,n} = 2T_n - T_Z$$

In Equation (6), T_n is the one-way travel time from the source to the reflector and T_Z is the one-way travel time from the source to the geophone location. Notice that when $Z \longrightarrow 0$, equivalent to the surface seismogram, then,

$$T_{o,n} \longrightarrow 2\,T_n \tag{7}$$

$$V_{RMS}(T_R) \longrightarrow V_{RMS}(T_n)$$

Substituting Equation (7) into Equation (4), we can see that dynamic time correction for the shot offset distance is the same as the conventional NMO correction. When $T_Z \longrightarrow T_n$, then

$$V_{RMS}(T_R) \longrightarrow V_{RMS}(T_Z) \tag{8}$$

Equation (8) with Equation (4) can be used for the dynamic time correction for the downgoing waves.

In order to apply dynamic time correction to the far-offset VSP data, the interval velocities must be known. The interval velocities of the media can be derived in the following way using the transmitted body wave of the VSP data.

Assuming horizontally layered and isotropic media, the travel time from the source to the top of the layer n can be written as (see Figure 15):

$$\bar{T}_n = \sum_{i=1}^{n} \frac{H_i}{V_i \sqrt{1 - P_n^2 V_n^2}} \tag{9}$$

$$l = \sum_{i=1}^{n} \frac{P_n V_i H_i}{\sqrt{1 - P_n^2 V_i^2}}$$

where $\bar{T}_n$ = transmitted arrival time,

l = offset distance,

V_i = medium velocity in the layer i,

H_i = thickness of the layer i, and

P_n = ray parameter.

The ray parameter P_n is related to Snell's law by

$$\frac{\sin\Theta_{in}}{V_i} = \frac{\sin\Theta_{nn}}{V_n} = P_n \text{ for } i=1, 2, \text{----}, n.$$

where Θ_{in} is the incidence angle at i-th interface for the ray from the source to n-th interface.

Using the first arrival times of the transmitted body waves and the geometry of the VSP configuration, we can estimate the medium velocity by solving Equation (9) iteratively. This may be done as follows.

Define superscript k to denote the k-th iterative solution. Then,

$$\bar{T}_n^{k+1} = \bar{T}_n^k + \frac{\partial \bar{T}_n^k}{\partial P_n^k}(P_n^{k+1} - P_n^k) + \frac{\partial \bar{T}_n^k}{\partial V_n^k}(V_n^{k+1} - V_n^k)$$

$$l^{k+1} = l^k + \frac{\partial l^k}{\partial P_n^k}(P_n^{k+1} - P_n^k) + \frac{\partial l^k}{\partial V_n^k}(V_n^{k+1} - V_n^k)$$

Using least square method, the iterative solution can be written in the matrix notation as:

$$[Y^{k+1}] = [M^k]^{-1} [Q_o] - [\bar{Q}^k] + [Y^k]$$

where $[Y^k] = \begin{bmatrix} P_n^k \\ V_n^k \end{bmatrix}$

$$[\bar{Q}^k] = \begin{bmatrix} \bar{T}_n^k \\ l^k \end{bmatrix}$$

and $[Q_o] = \begin{bmatrix} T_n^o \\ l \end{bmatrix}$ (10)

$$[M^k] = \begin{bmatrix} M_{11}^k & M_{12}^k \\ M_{21}^k & M_{22}^k \end{bmatrix}$$

T_n is the observed travel time and l is the offset distance, which is constant for all observations. The matrix element M, evaluated at the k-th iteration, is given by:

$$M_{11}^k = \sum_{i=1}^{n} \frac{H_i V_i P_n}{(1 - P_n^2 V_i^2)^{3/2}}$$

$$M_{12}^k = \frac{-H_n(1 - 2 P_n^2 V_n^2)}{V_n^2 (1 - P_n^2 V_n^2)^{3/2}}$$

$$M_{21}^k = \sum_{i=1}^{n} \frac{V_i H_i}{(1 - P_n^2 V_n^2)^{1/2}}$$

$$M_{22}^k = \frac{P_n H_n}{(1 - P_n^2 V_n^2)^{3/2}}$$

Therefore, using Equation (10), we can estimate medium interval velocities successively from the VSP section.

Figure 16a shows vertical component data acquired at MWX 2 well. Figure 16b shows the processed version of Figure 16a. The additional processing steps applied to Figure 16a to produce Figure 16b are:

1. velocity filtering to suppress S-wave arrivals,
2. downgoing wave train deconvolution to enhance vertical resolution,
3. dynamic time correction to compensate the source offset distance,
4. cumulative summation to enhance signal-to-random noise ratio, and
5. merging of downgoing waves and upgoing waves after boosting the amplitude of the upgoing waves by a factor of 3.

The importance of dynamic time correction in simulating zero-offset VSP section from the far-offset data is shown by this example.

DISCUSSION OF DATA

The standard field format of the MDS 10 recording system has only one end of file (EOF) mark between the record header and multiplexed data set. Unfortunately, the recorded field tape had an average of three inter-record gaps (IRG's) inside a data set. Standard demultiplexing programs cannot properly demultiplex data in the trace order when there are IRG's. Therefore, a lot of time was spent to recreate the gapless tape from the gapped field tape using a Fortran program compatible to the Phoenix I data processing system. During this process, about 4 to 8 samples were lost for each trace. Because the recorded sampling rate was 0.5 ms, the possible time error for the demultiplexed data is in the range of 2 to 4 ms.

The strength of a 450 $in.^3$ surface airgun source was adequate to profile the VSP data from 8,000 ft to the surface at this area. The original unstacked data shown in figure 3 reveals that the background noise before the onset of the downgoing wave is almost negligible. A similar plot for the far-offset vertical component VSP data also supports this observation.

Figure 7 shows the high amplitude ringing of the initial downgoing waveform. Near-surface reverberation could affect this long-time history of the downgoing waves. However, the other cause of this phenomenum could have been from the result of three elements of the airgun not being properly synchronized. The monitor-phone records, shown in figures 4 and 5, show three prominent peaks, which could have been the effect of nonsynchronization of three elements in the airgun. Due to this nonsynchronization of the airgun, the overall frequency content of the VSP data could have been reduced.

The primary reflection amplitude generated around 8,000 ft, which is shown in figure 10 with an arrow, was very weak compared with the VSP section without downgoing wave train deconvolution. The detailed analysis showed that the reverberation pattern of the downgoing wave above 6,275 ft was substantially different from that below 6,275 ft. The reason for this was the source location was changed at the depth level of 6,275 ft. Upgoing wave character changes due to the source location change is clearly seen at the depth level of 6,275 ft on figure 8. Therefore, the deconvolution operator designed at the depth level of 3,025 ft would not work properly for the data set below 6,275 ft.

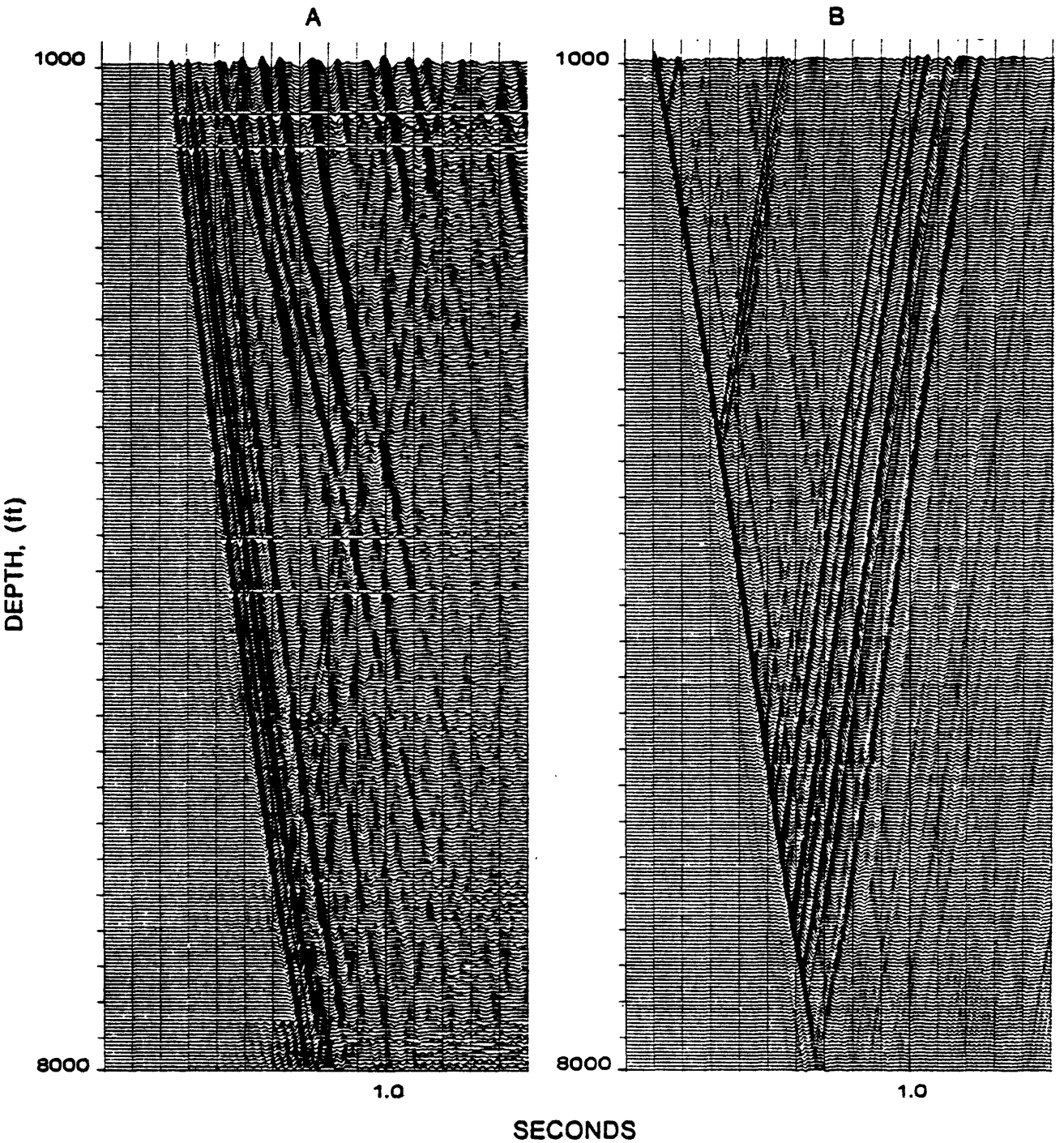

Figure 16.--Comparison between unprocessed and processed far-offset VSP data at MWX 2 well. (A) Unprocessed VSP data with trace interval of 25 ft; (B) processed VSP data.

To compensate for the effect of the source location change on the seismic character, the section shown in figure 10 was deconvolved again using an average downgoing wavelet around 6,200 ft. The result is shown in figure 17. The reflected event with an arrow mark, shown in figure 17, is well enhanced. There are some subjective matters in designing downgoing wave train deconvolution operator and application. Each designing criterium and application should be incorporated with the specific objectives of VSP data.

The substantial change of downgoing waveform due to the source location change (in the order of 20 ft) was also discussed by Balch and others (1982). Sometimes source location changes are troublesome in the processing and interpretation of VSP data. Some of the effects can be reduced during the processing stage by either a shaping-filter approach or a deconvolution technique. However, it is important to keep the source location changes to a minimum during the field operation to get better results.

The oriented in-line horizontal component data at the MWX 2 well from the far-offset source are shown in figure 18. The upgoing waves are boosted by a factor of 3 compared to the downgoing waves in order to see the detailed structure of the upgoing waves. This figure indicates that the surface airgun source generated a substantial amount of shear waves. Also the mode conversion at the boundary can be clearly observed in figure 18. The longitudinal to vertically polarized shear wave mode conversions are well defined at the depths of approximately 3,800 ft and 7,000 ft. The presence of shear waves on the VSP section has advantages and disadvantages in interpreting the VSP data. Most of the disadvantages could be handled by careful processing. The advantage should be fully utilized in the interpretation of VSP data.

Also observe that the downgoing shear waves are very weak below 7,400 ft on figure 18. Original records show a high level of ambient noise, possibly caused by poor downhole geophone coupling to the borehole wall. Log analysis indicates that there are abundant coal beds with thicknesses varying from 10 to 30 ft in the depth range of 6,600 to 7,500 ft. Therefore, the weak shear wave amplitudes observed below 7,400 ft could be caused by either the poor geophone coupling or high transmission losses of shear waves due to the abundant coal beds, or both effects.

INTERPRETATION

Identification of Reflected Events

Figure 19 shows the cumulative summed vertical component of upgoing waves of the MWX 2 well from a near-offset VSP data set. This cumulative upgoing wave at the shallow depth is very similar to the stacked surface seismic data around a borehole. In order to identify the depth origins of the reflected events shown in figure 19, the upgoing waves are merged together with the downgoing waves. The result is shown in figure 20. From figure 20, the origin of the reflectors can be identified by carefully mapping the intersection points betweeen the downgoing waves and the upgoing waves. The identified zones of interest are shown in the figure.

Figure 21 shows the detailed view of the reflected events below the fluvial zone. The data shown in figure 21 came from the vertical component of VSP data at the MWX 2 well from the far-offset source. In this figure, reflections from near the top of the Rollins Sandstone and Cozzette Sandstone within the marine zone are also indicated.

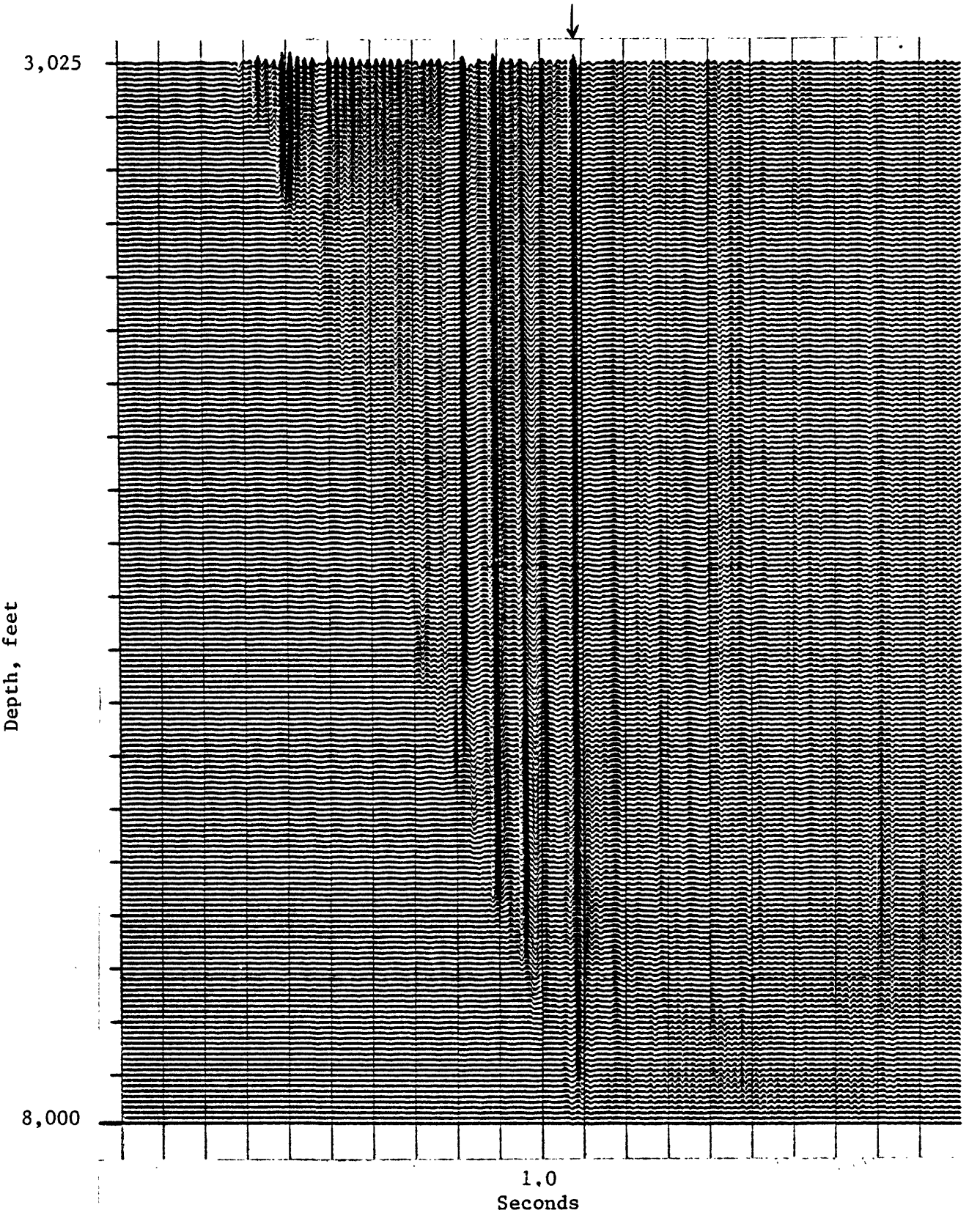

Figure 17.--Cumulative-summed, vertical component upgoing wave deconvolution. The downgoing wave deconvolution operator was designed around the depth level of 6,200 ft and this operator was applied to the data shown in figure 10.

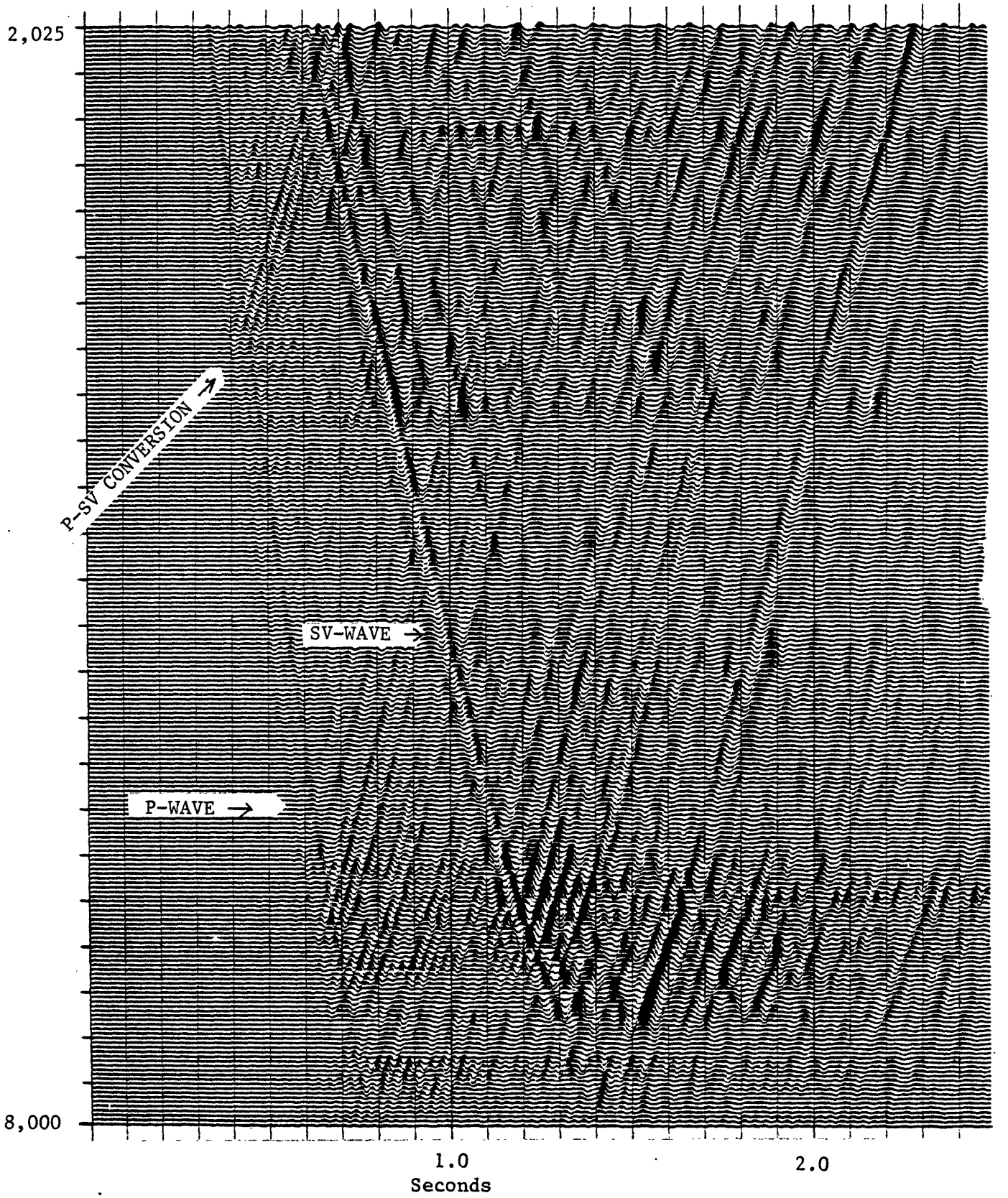

Figure 18.--In-line, horizontal-component data at MWX 2 well from the far-offset source.

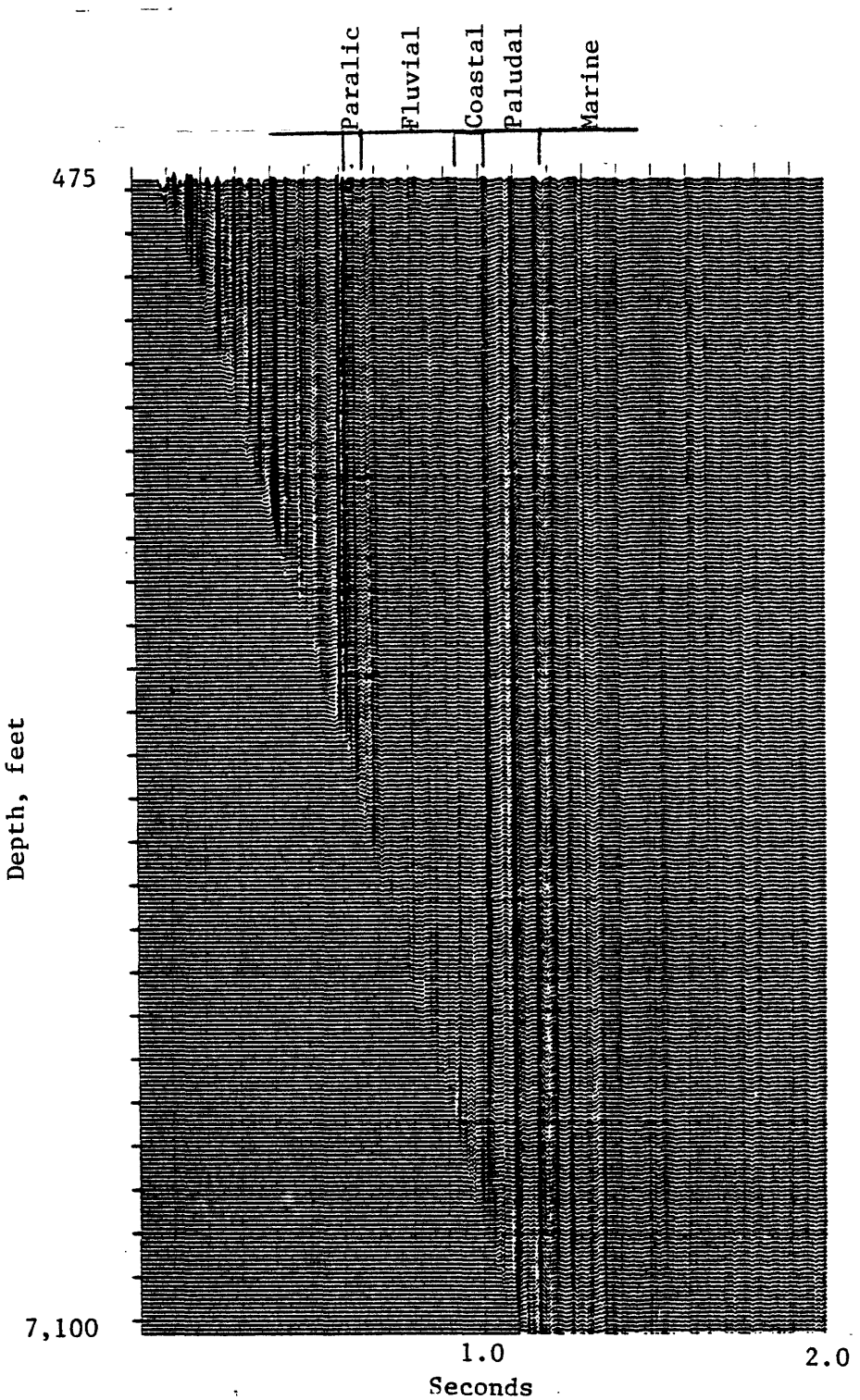

Figure 19.--Cumulative-summed, vertical-component upgoing waves at MWX 2 well from the near-offset source. Interpreted zones are shown at the top of the figure.

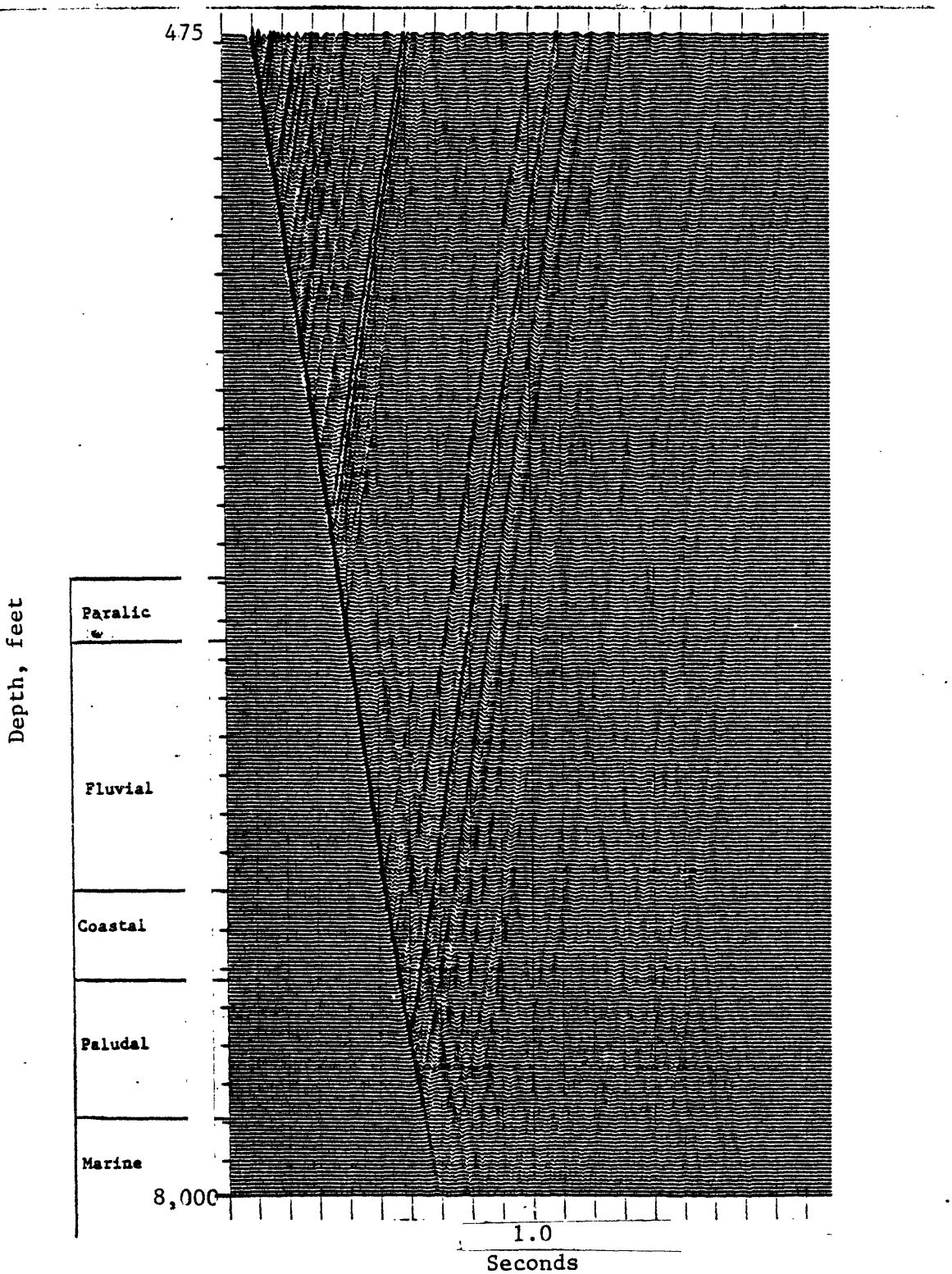

Figure 20.--Merged downgoing and upgoing waves at MWX 2 well from the near-offset source. Interpreted zones are shown at the side of the figure.

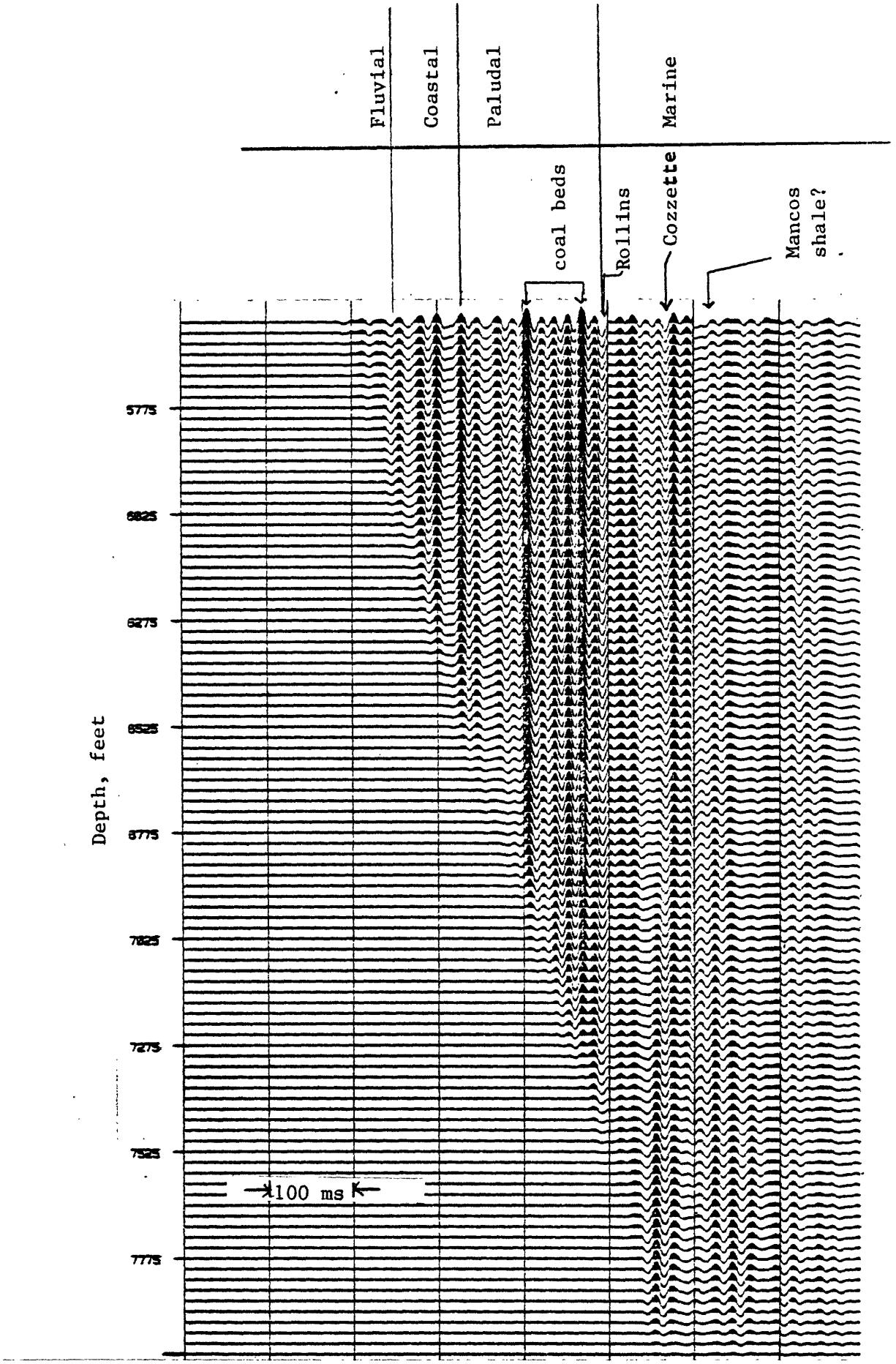

Figure 21.--Cumulative-summed, vertical-component upgoing waves at MWX 2 well from the far-offset source. Interpreted zones are shown at the top of the figure.

To identify shear wave (SH-wave) reflections, the transverse component of VSP data at the MWX 2 well from the far-offset source were used. Figure 22 shows the cumulatively summed upgoing shear waves with the downgoing waves. The interpreted zones are shown in the figure.

The identification of the reflected events from the VSP data section is simple compared to the surface seismic data as shown in these examples.

Due to the lack of high frequency content of the VSP data, it was not possible to resolve individual small sand bodies or coal beds. The seismic events shown in figures 19 through 22 are the total seismic responses of many closely spaced beds. Figure 23 shows the effect of frequency content of the input wavelet with respect to the bed thickness and vertical distribution of the beds. Figure 23a shows the one-dimensional model result using 25 Hz Ricker wavelet for the coal beds in the paludal zone, and figure 23b shows the same model with 80 Hz Ricker wavelet. The horizontal spikes on figure 23 show the individual reflection coefficient at the bed boundary; light, dotted and continuous lines represent the individual responses of each boundary; and the heavy, continouous line represents the total response of the model. Even the 80 Hz Ricker wavelet (figure 23b) cannot resolve the individual coal beds. The seismic response of the 25 Hz Ricker wavelet is very similar to that of VSP data shown in figure 21.

Seismic Characters

Figure 24 shows the cumulative summed vertical component of upgoing waves at the MWX 1 well from the near-offset source with various band-pass filters. The relatively large amplitude reflected events characterizes the seismic events from the paludal and marine blanket sandstone and coal bed interferences within the paludal zone. The reflection amplitudes from the coastal zone are relatively low compared to the paludal zone. The upper fluvial zone consists of high frequency and high amplitude reflection events, but the lower fluvial zone is characterized by a very quiet seismic zone.

The narrow band-pass filtered (20/26 - 34/40 Hz) upgoing waves, the bottom plot of figure 24, shows only severe interference peaks and troughs. The seismic character within the frequency range of 20/26 - 34/40 Hz from the paludal zone is very similar to the one-dimensional model result shown in figure 23a, and is very similar to the 3-D high resolution surface seismic data, which were acquired and processed by Colorado School of Mines (written commun. with Fried, 1982).

Figure 25 shows the same plot as figure 24 for the MWX 2 well. The seismic characters of the paludal and marine zones are very similar to those of the MWX 1 well. However, the seismic character of the fluvial and coastal zones appear to be remarkably different between the two wells, which are only approximately 130 ft apart, even if the differences in the processing noise and the geophone coupling between the two wells is considered. One of the reasons for the observed differences between the two wells could be the effect of the differences in the acoustic properties of the beds, and spatial distribution of the beds. The fluvial and coastal zones mainly consist of the small lenticular-type sand bodies, while the paludal and marine zones consist of the large blanket sandstones and coal beds.

In the case of the small lenticular-type sand bodies, when compared to the dominant wavelength considered, the effect of the diffractions from the edges of the body could alter the reflection characters of the sand body.

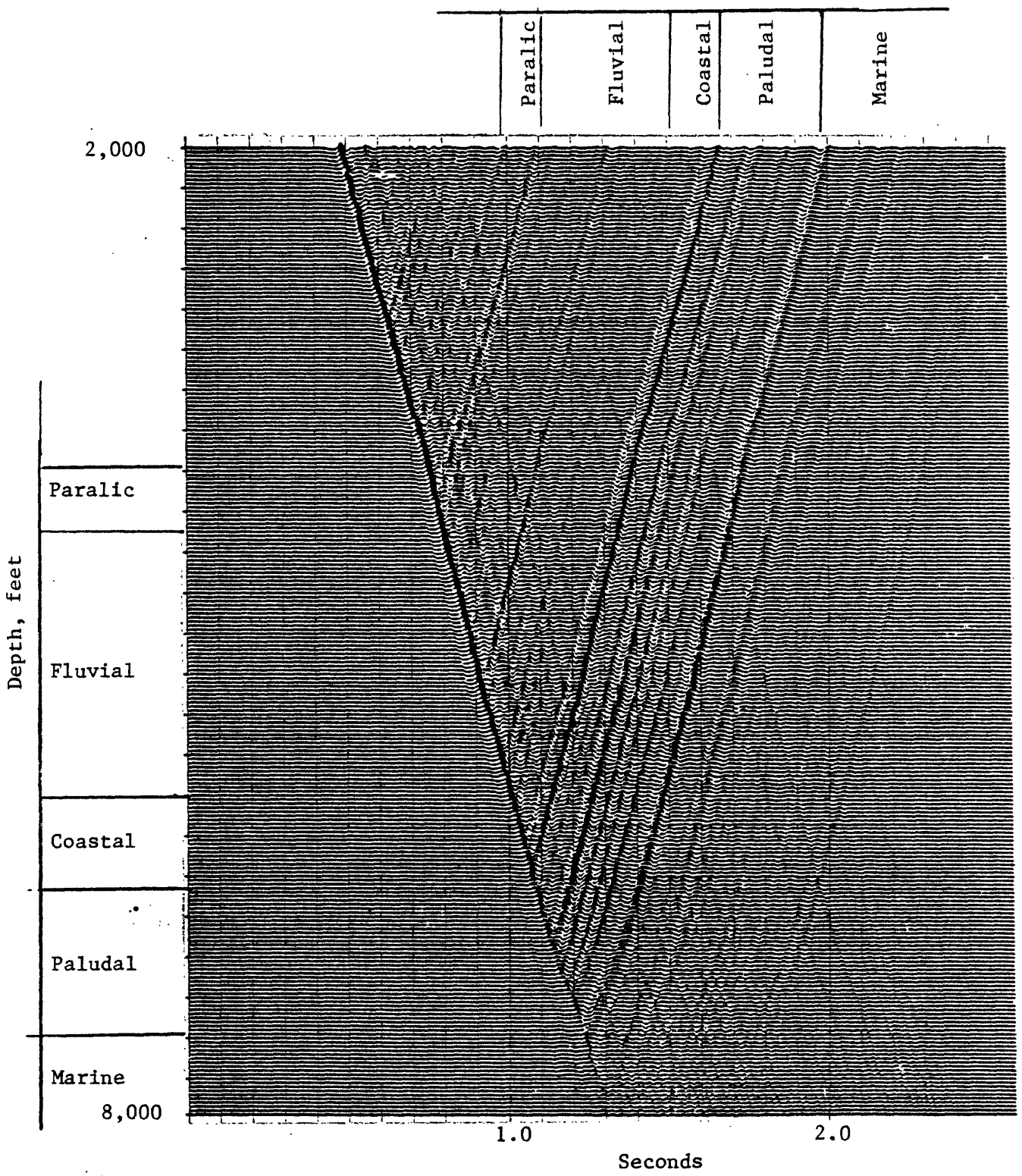

Figure 22.--SH-waves at MWX 2 well from the far-offset source. Interpreted zones are shown at the side of the figure.

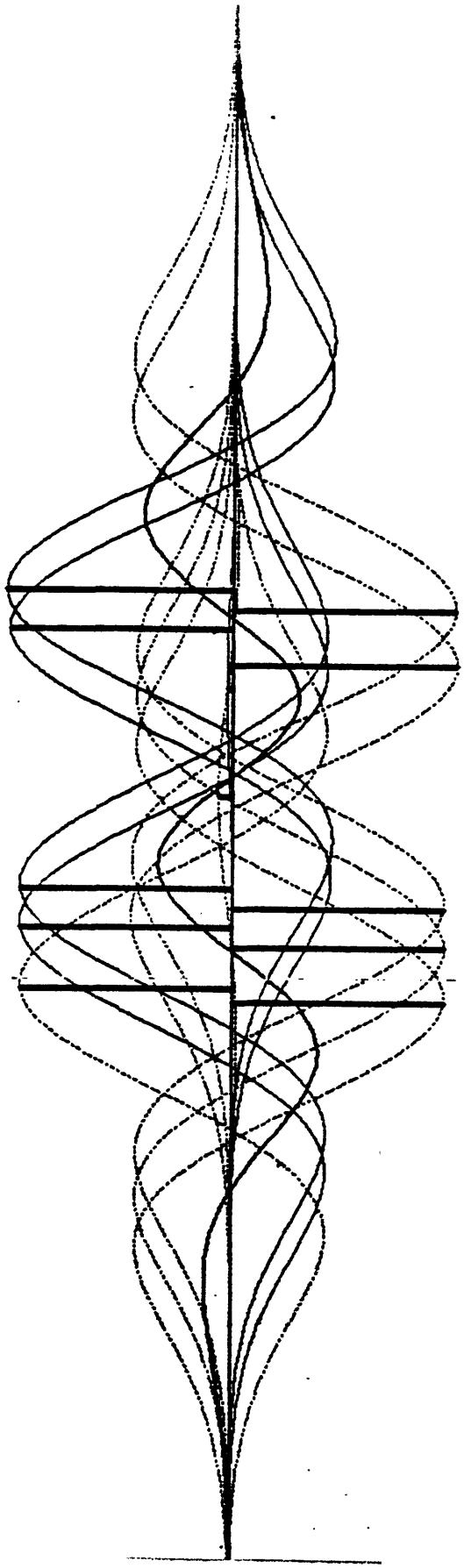

Depth, feet	Density g/cm^3	Velocity ft/msec
	ρ = 2.5	V = 12,250
6,764		
	ρ = 1.3	V = 7,200
6,770		
	ρ = 2.5	V = 12,000
6,780		
	ρ = 1.3	V = 7,200
6,790		
	ρ = 2.8	V = 10,800
6,800		
	ρ = 2.55	V = 11,600
6,850		
	ρ = 2.53	V = 11,000
6,890		
	ρ = 1.3	V = 7,200
6,896		
	ρ = 2.43	V = 11,000
6,904		
	ρ = 1.3	V = 7,200
6,910		
	ρ = 2.53	V = 11,000
6,928		
	ρ = 1.3	V = 7,200
6,932		
	ρ = 2.53	V = 11.000

Figure 23a.--One-dimensional seismic modeling for the coal beds in the paludal zone at MWX 2 well. Model parameters are shown in the figure. (a) Using 25 Hz Ricker wavelet.

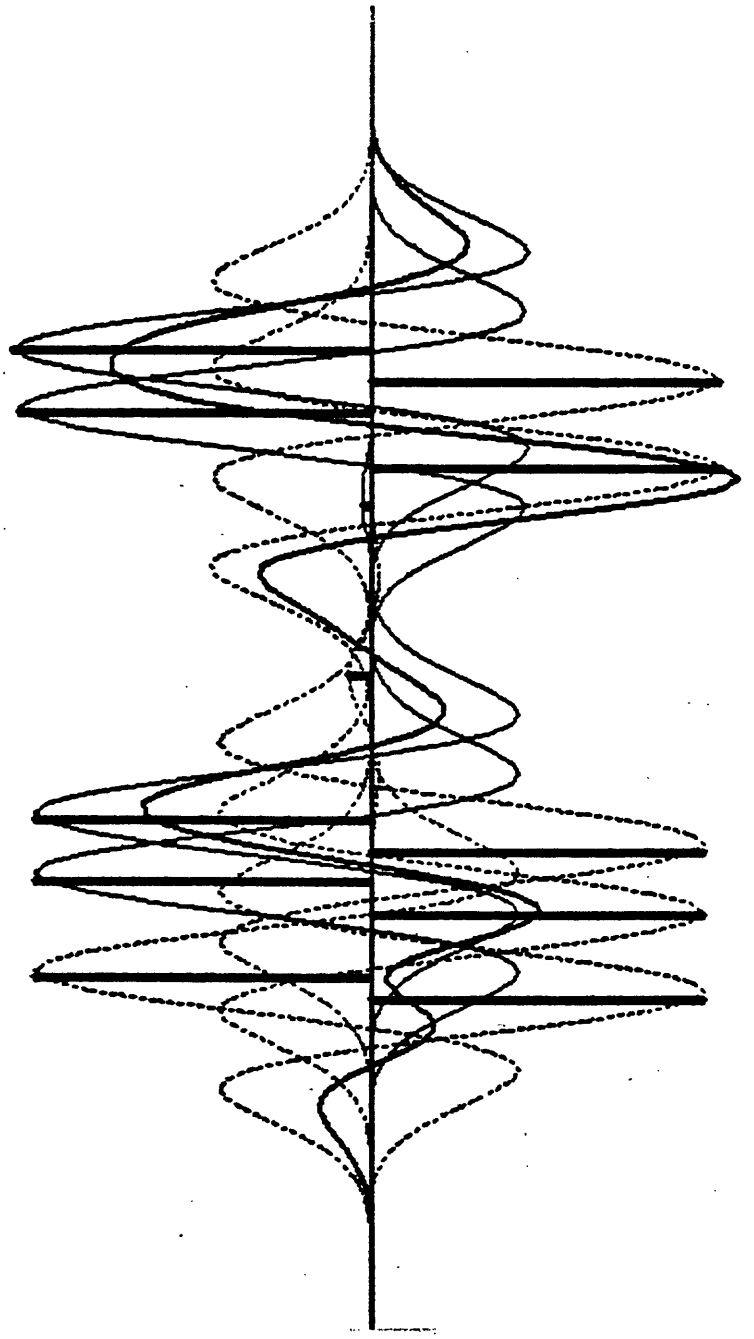

Depth, feet	Density g/cm^3	Velocity ft/msec
	ρ = 2.5	V = 12,250
6,764		
	ρ = 1.3	V = 7,200
6,760		
	ρ = 2.5	V = 12,000
6,780		
	ρ = 1.3	V = 7,200
6,790		
	ρ = 2.8	V = 10,800
	ρ = 2.55	V = 11,600
6,850		
	ρ = 2.53	V = 11,000
6,890		
	ρ = 1.3	V = 7,200
6,896		
	ρ = 2.53	V = 11,000
6,904		
	ρ = 1.3	V = 7,200
6,910		
	ρ = 2.53	V = 11,000
6,928		
	ρ = 1.3	V = 7,200
6,932		
	ρ = 2.53	V = 11,000

Figure 23b.--One-dimensional seismic modeling for the coal beds in the paludal zone at MWX 2 well. Model parameters are shown in the figure. (b) Using 80 Hz Ricker wavelet.

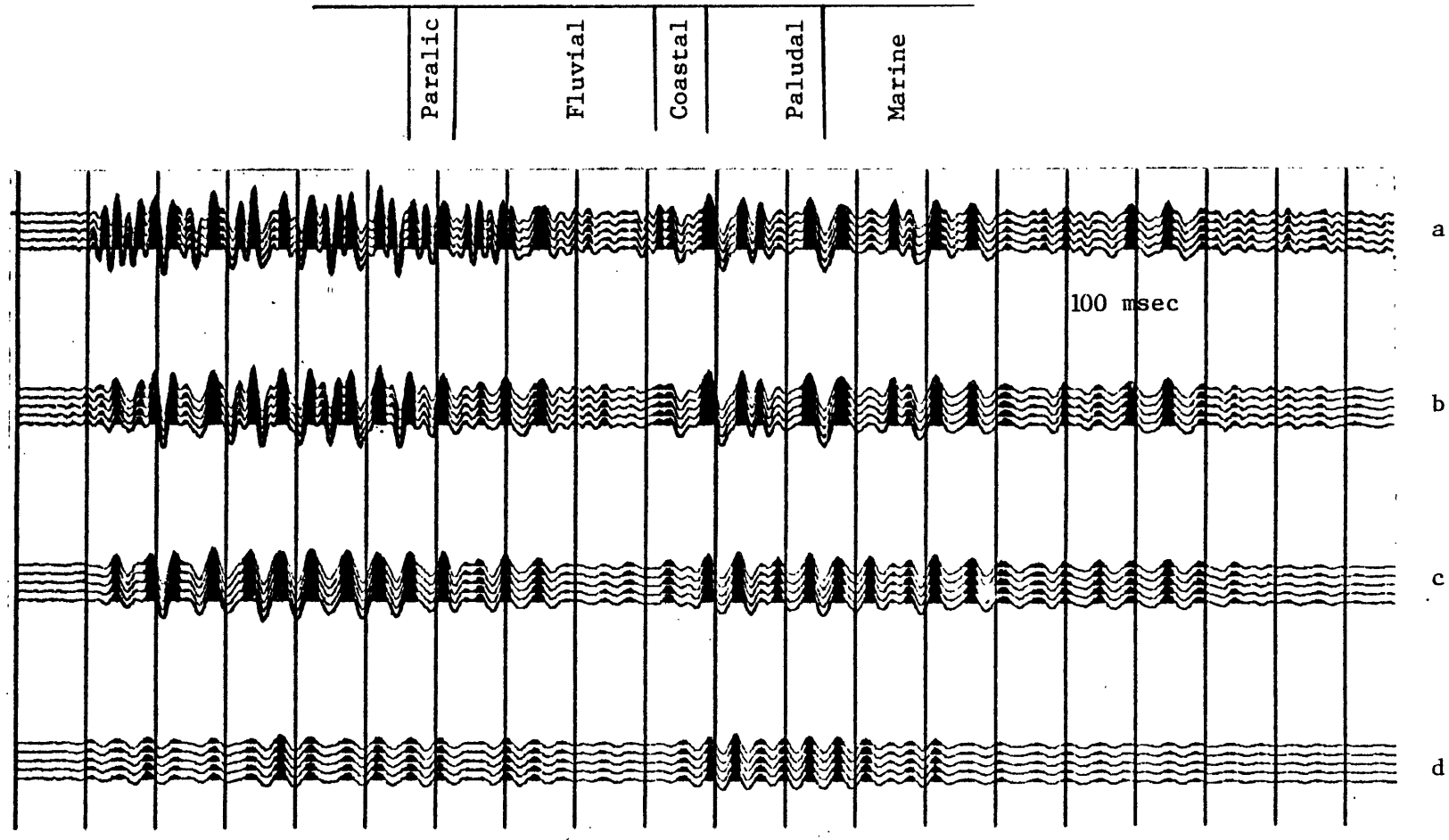

Figure 24.--Vertical-component upgoing wave at MWX 1 well from the near-offset source with various band-pass filters. (a) 4/8-64/76 Hz; (b) 8/12-48/58 Hz; (c) 15/20-35/45 Hz; (d) 20/26-34/40 Hz.

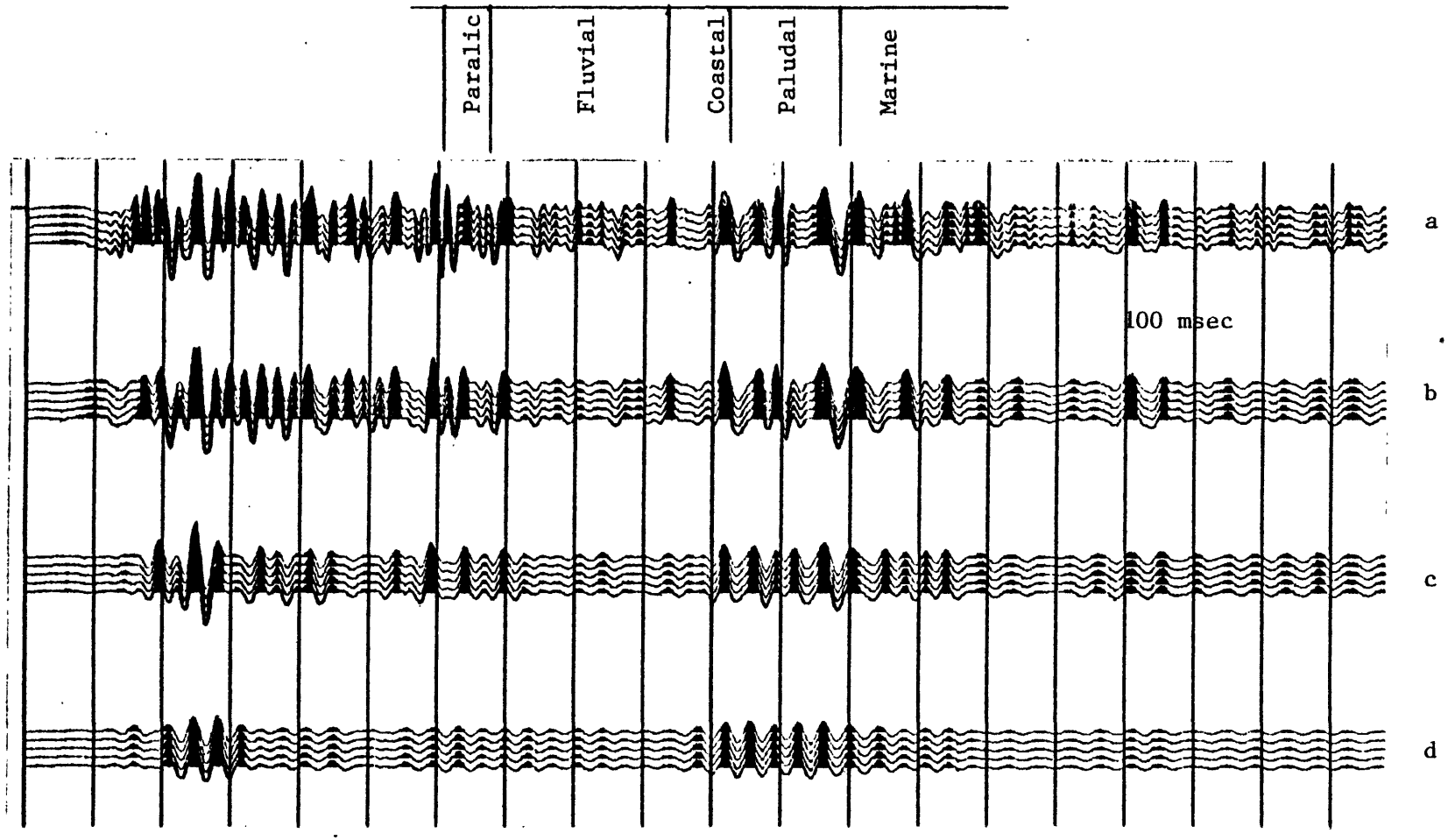

Figure 25.--Vertical-component upgoing wave at MWX 2 well from the near-offset source with various band-pass filters. (a) 4/8-64/76 Hz; (b) 8/12-48/58 Hz; (c) 15/20-34/40 Hz; (d) 20/26-34/40 Hz.

Log and core analyses of the two wells, MWX 1 and MWX 2, indicate that most of the sand bodies in the fluvial and coastal zone do not intersect the borehole at the same depth, which implies that the small sand bodies could be randomly distributed throughout this experimental area.

The amount of the diffraction effect on the seismic amplitudes with respect to the size of the sand bodies is not known at the present time. However, the differences of the seismic amplitude between two wells for the fluvial and coastal zones could be due to the effect of the random spatial distribution of the small lenticular-type sand bodies in this area.

Figure 26 shows the cumulative summed vertical component reflected events at the MWX 2 well from the far-offset source. There are some differences in the seismic character for the paludal and marine zones compared with those in figure 25. However, the differences of the seismic characters in the fluvial and coastal zones with respect to the source distance are quite substantial.

One possible interpretation of this observation could be the effect of the configuration of the spatial distribution of the lenticular-type sand bodies around the well. The analysis of the seismic character differences with respect to the source location could provide pertinent information for delineating the spatial distribution of the sand bodies.

Figure 27 shows the correlations at the MWX 2 well between vertical component P-wave from the near-offset VSP data and horizontal component SH-wave from the far-offset VSP data. The primary objective of correlating P-wave and SH-wave recorded from two different source locations was to examine the errors introduced during the processing stage. The overall seismic responses of the P-wave are very close to those of the SH-wave, which implies a high level of confidence in both P-wave and SH-wave data.

More detailed reflection character and relatively large amplitudes are observed from the SH-wave data than from the P-wave data. The reasons for the seismic character change between P- and SH-wave reflected events could be as follows.

1. Acoustic property change due to the fracturing of the sand body could have more effect on the S-wave than on the P-wave. Albright and others (1980) showed that fracturing has a more pronouced effect on the S-wave than on the P-wave. Consequently, the reflections from the fractured sand bodies could have higher amplitude in the SH-wave than in the P-wave. The large amplitude shear wave reflection within the fluvial zone corresponds roughly to the position of the fractured zone on the well logs and in the cross borehole survey (Searls and others, 1983).

2. Effective wavelength of the SH-wave might be less than that of the P-wave. The shorter the wavelengths become, the better the resolution.

In order to increase the spatial and vertical resolution, a high frequency content of the seismic data is needed. Even though the high frequency content of the data is constrained by the earth attenuation and seismic source characteristics, some of the high frequencies can be recovered by the processing.

Figure 28 shows the detailed correlation below the fluvial zone between P-wave and SH-wave at the MWX 2 well from the far-offset source. The data shown in figure 28 are the results of reprocessing VSP data at the MWX 2 well in order to increase the frequency content of the data for the intervals below the fluvial zone. The correlations are excellent and the resolutions are better compared to the data shown in figures 26 and 27. This figure also reveals that SH-wave provides better resolution. This analysis indicates that even though shear wave suffers more earth

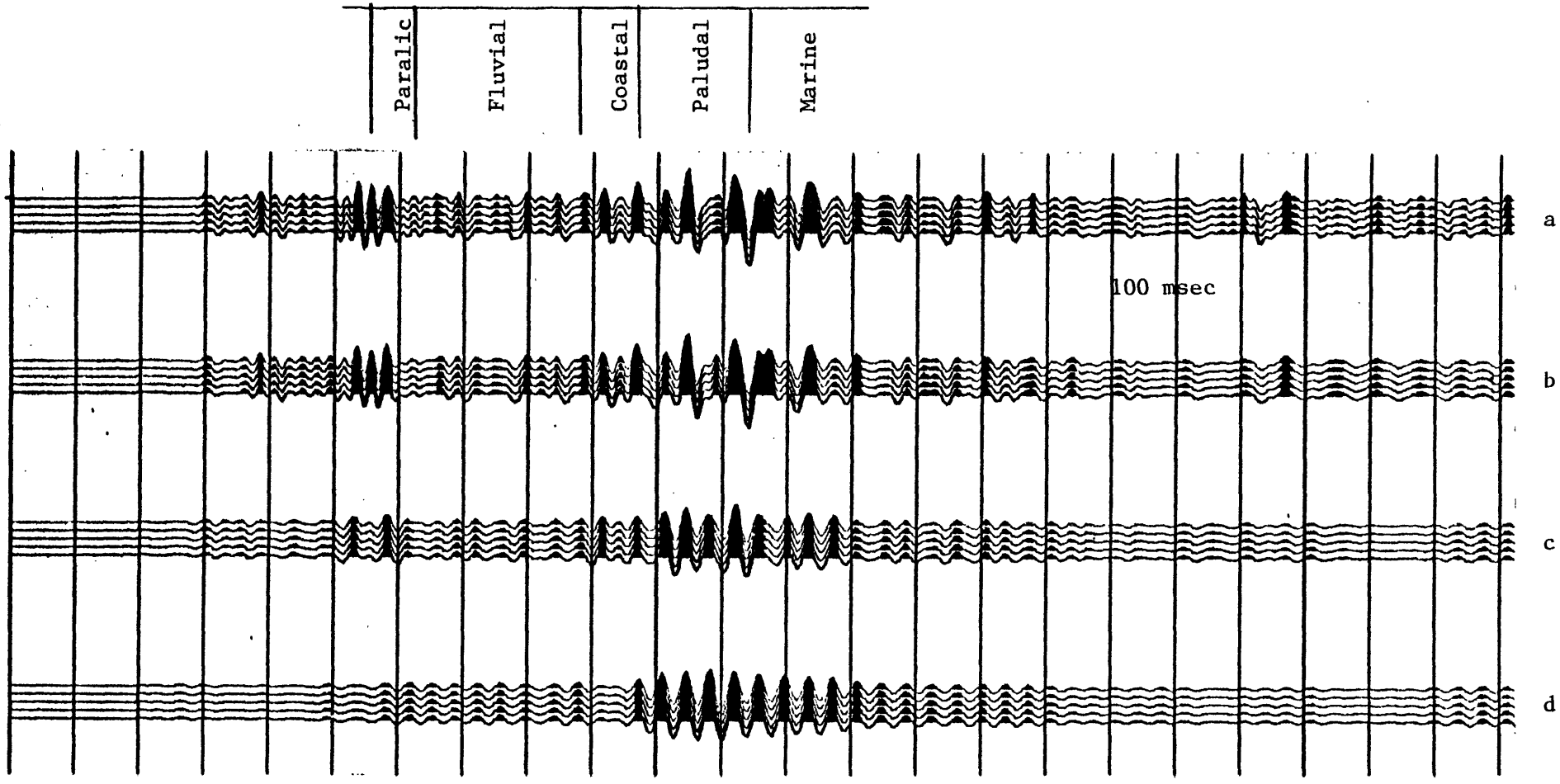

Figure 26.--Vertical-component upgoing wave at MWX 2 well from the far-offset source with various band-pass filters. (a) 4/8-64/76 Hz; (b) 8/12-48/58 Hz; (c) 15/20-35/45 Hz; (d) 20/26-34/40 Hz.

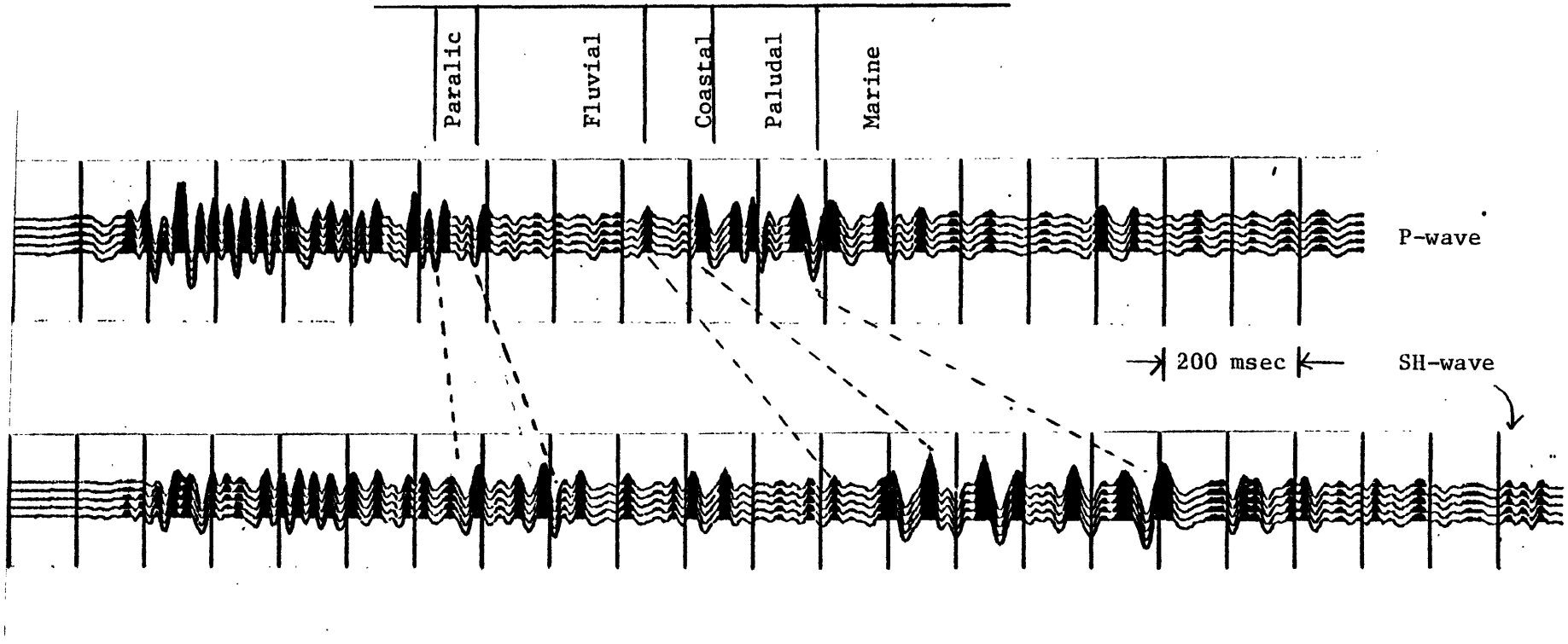

Figure 27.--Correlation between P- and SH-waves at MWX 2 well. The top portion is the vertical-component upgoing wave from the near-offset source and the bottom portion is the horizontal (transverse) component upgoing wave from the far-offset source.

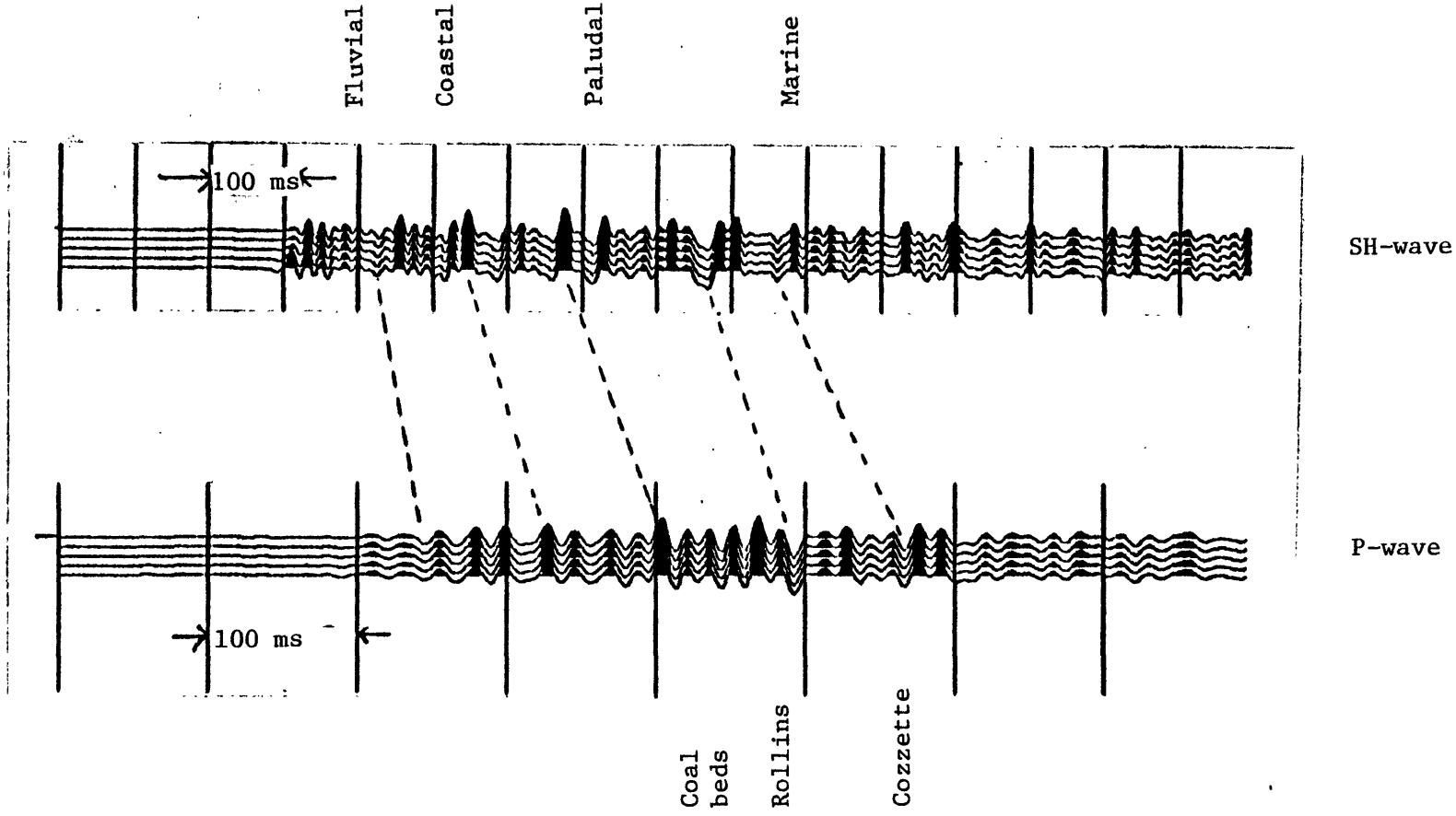

Figure 28.--Detailed correlation between P- and SH-waves at MWX 2 well from the far-offset source.

attenuation, the resolution of S-wave could be better than the resolution of P-wave at this area. This conclusion could also be applied to the surface seismic data.

Acoustic Parameters

Theoretically, the important acoustic parameters--such as velocity, density, and attenuation--can be estimated by VSP data from a surface source. However, accuracy and resolution are limited largely by the frequency content of the VSP data.

Estimation of the interval velocity is discussed in detail in the processing part. Figure 29 shows the estimated P- and SH-wave interval velocities averaged over 125 ft from the VSP data at the MWX 2 well. Remarkably low interval velocities at the depth around 7,000 ft to 7,400 ft are due to the presence of abundant coal beds. The detailed correlation between P- and SH-wave interval velocities may not be made mainly due to the large wavelength involved in estimating velocities. However, the general velocity distribution with depth is in good agreement.

Knowing P- and S-wave velocities, Poisson's ratio (σ) can be derived by the following formulae:

$$\sigma = \frac{1-2V_\beta^2/V_\alpha^2}{2(1-V_\beta^2/V_\alpha^2)} \triangleq \frac{1-2r}{2(1-r)}$$

where

$$r = \frac{V_\beta^2}{V_\alpha^2} \tag{11}$$

where V_α is the P-wave velocity and V_β is the S-wave velocity.

Poisson's ratio at the MWX 2 well is shown also in figure 29. The accuracy of Poisson's ratio depends on the accuracy of the estimated P- and S-wave velocities. Percentage error introduced to Poisson's ratio with respect to the percentage error in the velocities can be derived from Equation (11). The equation is:

$$\frac{\Delta\sigma}{\sigma} = \frac{2r}{(1-2r)(1-r)} \left(\frac{\Delta V_\alpha}{V_\alpha} - \frac{\Delta V_\beta}{V_\beta}\right) \triangleq \frac{2r}{(1-2r)(1-r)} \frac{\Delta V}{V} \tag{12}$$

Figure 30 shows the relation of Equation (12) for a given 10% total error in estimating velocity. This figure indicates that more than 20% error is introduced in Poisson's ratio when the true Poisson's ratio is greater than 0.3. Therefore, this kind of error analysis should be incorporated in the use of the estimated Poisson's ratio.

Bulk density information around a borehole can be estimated from the VSP data using tube wave and shear wave velocities. The tube wave velocity V_T in an open hole is given by (White, 1965)

$$V_T = \left\{ \frac{1}{V_f^2} + \frac{\rho_f}{\rho_s V_s^2} \right\}^{-1/2} \tag{13}$$

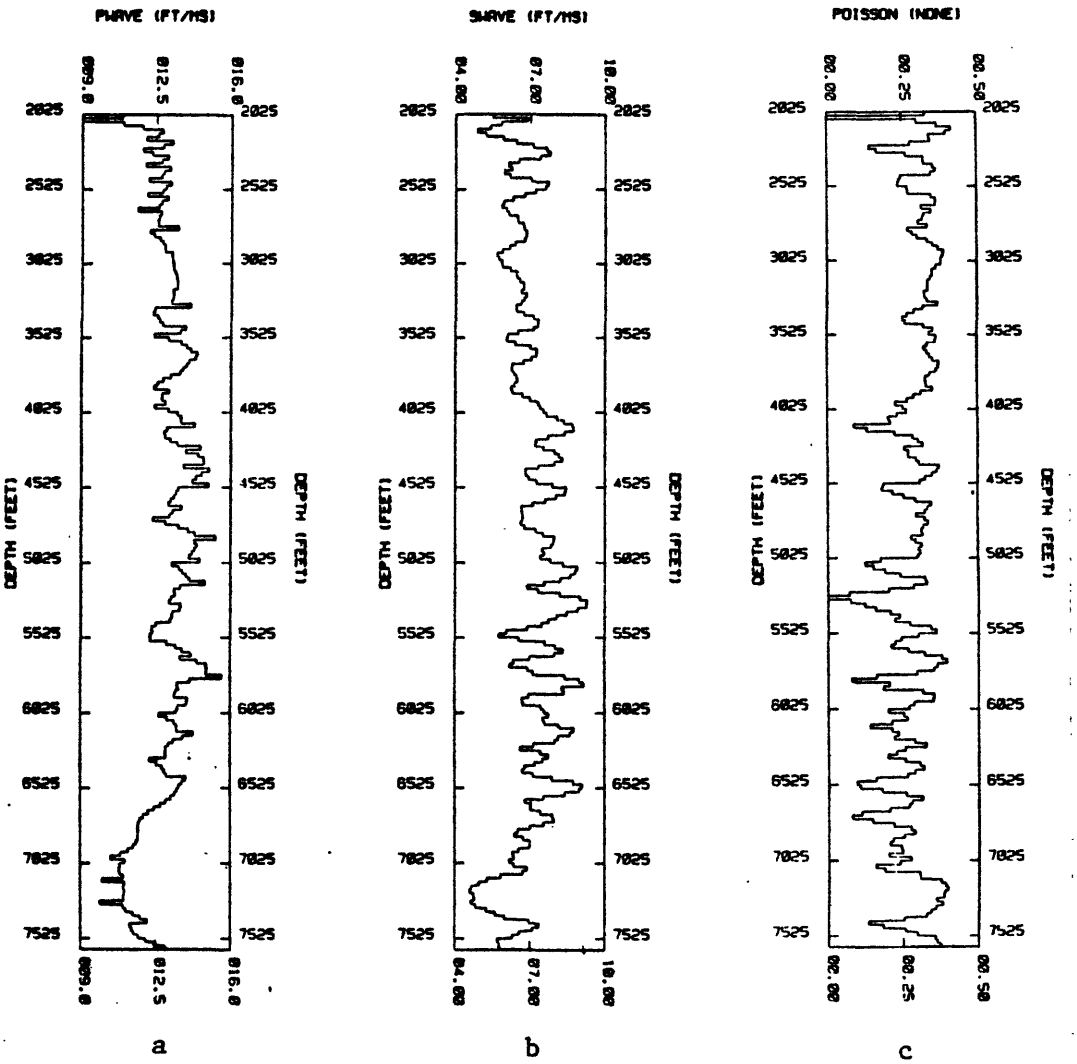

Figure 29.--Estimated acoustic parameters at MWX 2 well from the far-offset VSP data. (a) P-wave interval velocity; (b) S-wave interval velocity; (c) Poisson's ratio.

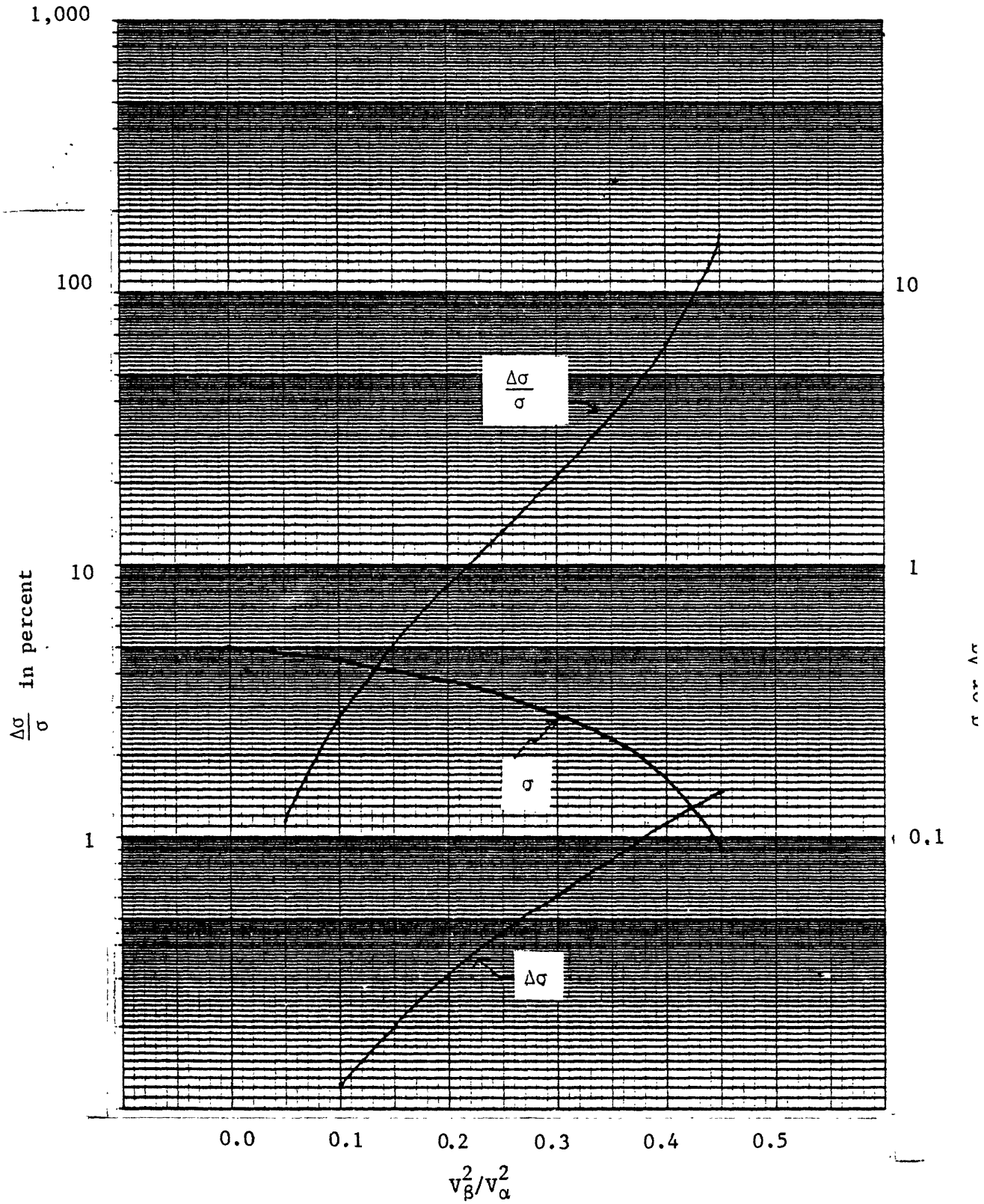

Figure 30.--The variation of the percentage error in estimating Poisson's ratio with respect to V_β^2/V_α^2 for a given velocity uncertainty, $(\Delta V_\alpha/V_\alpha - V_\beta/V_\beta) = 10\%$.

where V_f and ρ_f are the compressional velocity and density of the fluid respectively and ρ_s is the density of the surrounding solid. Therefore, with the estimated velocity V_ρ from figure 29 and the tube wave shown in figure 6, the bulk density around the MWX 2 well can be estimated.

The percentage error in estimating density with respect to the percentage error in the tube wave velocity can be written by the following equation using Equation (13).

$$\frac{\Delta\rho_s}{\rho_s} = \frac{-2\rho_s}{(1 - \frac{V_T^2}{V_f^2})} \left(\frac{\Delta V_T}{V_T}\right) \qquad (14)$$

Figure 31 shows the relation of Equation (14) with two values of $\Delta V_T/V_T$. This figure indicates that the accuracy of the tube wave velocity estimation should be less than 1% if maximum error in the estimating density is less than 20% for all values of V_T/V_f ratio. The dominant (troublesome) part of Equation (14) is the ratio V_T/V_f. Tube wave velocity in the cased hole is higher than the tube wave velocity in the open hole. So the accuracy in estimating tube wave velocity in the cased hole should be greater than in the open hole in order to have the same percentage errors in density.

An attempt has been made to study the feasibility in estimating bulk density using the tube wave velocity. Unfortunately, at the time of the analysis, open-hole tube wave velocity was used in estimating the bulk density while the hole was, in reality, cased. Therefore, the result of the bulk density estimation is excluded from this report. However, the study indicates that the bulk density around a borehole could be estimated by the method described here. The bulk density information might be used in estimating an average sand percentage around the MWX well site.

Finally, the P-wave attenuation was measured in order to provide some information for future field experiments. The downgoing P-wave and its amplitude spectrum at the depth level of 7,775 ft is shown in figure 32. Comparing the amplitude spectra at 3,025 ft, shown in figure 9b, the average apparent attenuation coefficient of P-wave can be estimated. In the frequency range of 10-70 Hz, the estimated apparent attenuation coefficient (Q) between 3,000 ft and 7,800 ft at the MWX 2 well is in the order of 40.

SUMMARY AND CONCLUSIONS

The strength of a single 450 $in.^3$ surface airgun was adequate in profiling the VSP data at the MWX well site near Rifle, Colorado. Low frequency content of the source signature was one of the disadvantages, but this can be improved by carefully synchronizing the airgun.

The malfunctioning of the horizontal component phones during most of the recording time degraded the final interpretation to a certain extent. The improvement of the horizontal component phones is highly desirable.

The primary objective of this investigation was accomplished. Based on the vertical component data at the MWX 1 and MWX 2 wells and the three-component data at MWX 2 well, the following conclusions can be made.

1. Reliable reflections were extracted from the VSP data and interpreted with a high level of confidence. The seismic signatures from the blanket sandstones and coal beds within the paludal and marine zones are

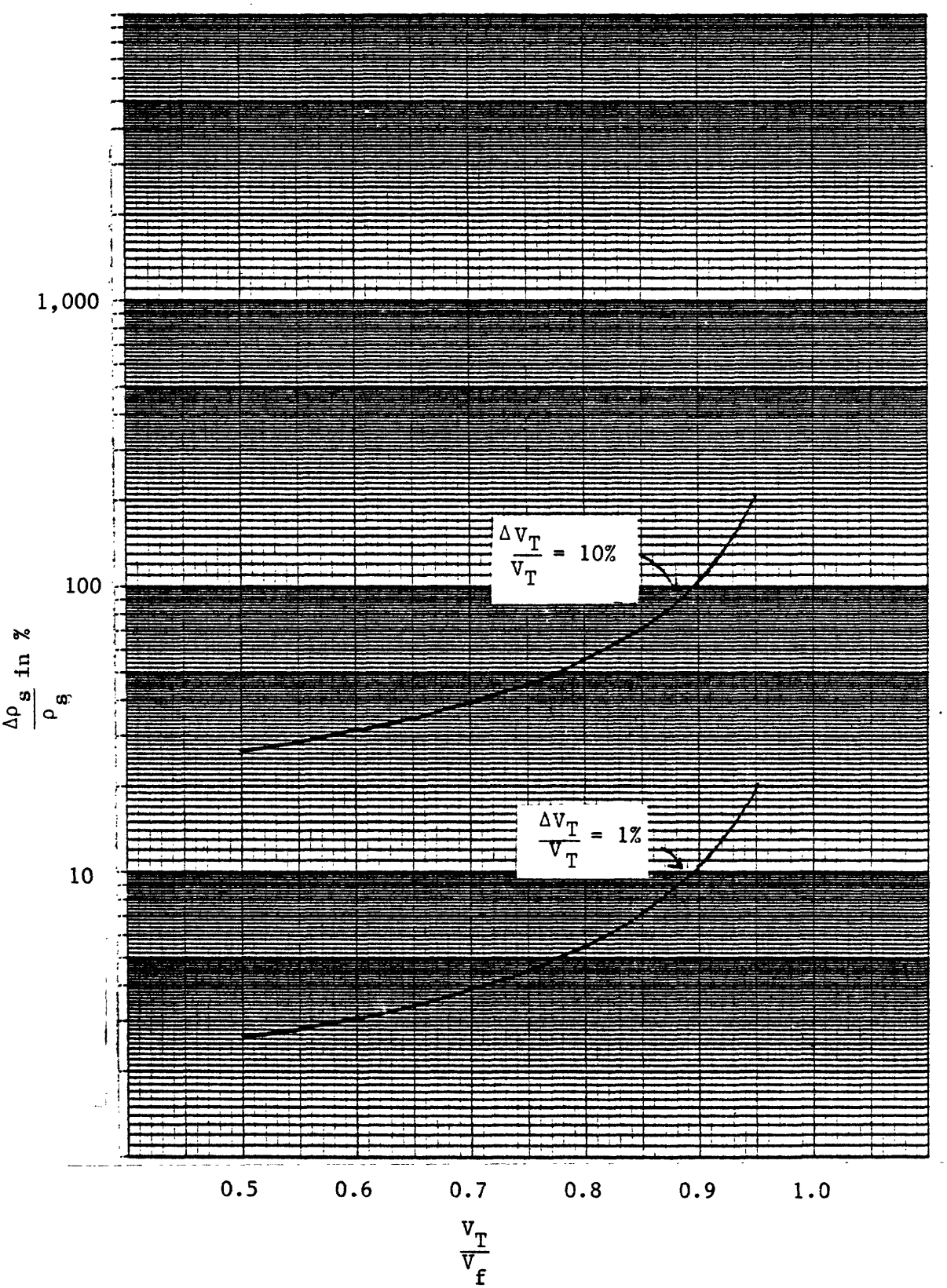

Figure 31.--The variation of the percentage error in estimating the bulk density using tube-wave velocities with respect to V_T/V_f.

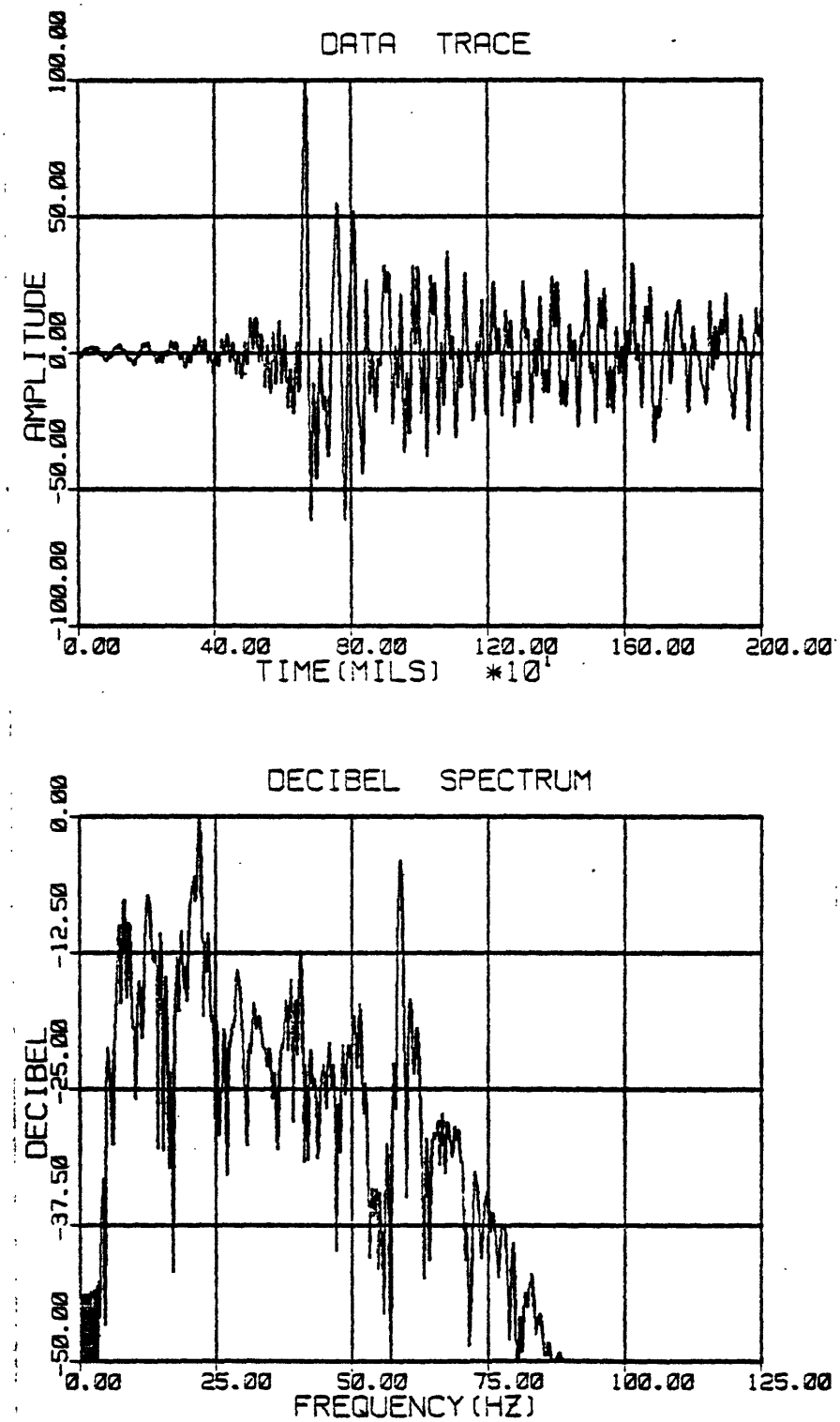

Figure 32.--Downgoing wave at MWX 2 well (top) and its amplitude spectrum (bottom) at the depth level of 7,775 ft after downgoing-wave deconvolution.

characterized by the high amplitude and continuous events on the VSP section. On the other hand, the seismic character of the lenticular-type sandstones within the fluvial and coastal zones are characterized by relatively small and discontinuous seismic events.

2. In addition to longitudinal-wave VSP data, highly reliable shear-wave VSP were also recorded by a surface source. Utilization of S-wave information with P-wave increases the exploration capability of the VSP method tremendously.

3. Seismic character differences from the lenticular-type sand bodies with respect to the source-offset distance could be applied to the delineation of the spatial distribution of sands.

4. Shear-wave VSP data indicate that the acoustic properties of the lenticular sand zone, particularly in the fractured zone, may represent large changes in shear modulas. This implies that the shear-wave survey may provide better results in detecting small lenticular-type sand bodies than the P-wave survey. Also the shear-wave survey may provide better vertical and spatial resolution than the P-wave, because the dominant wavelength of the S-wave could be less than that of the P-wave.

5. Acoustic properties such as P-wave velocity, S-wave velocity, Poisson's ratio, attenuation and bulk density can be estimated from the three-component VSP data.

RECOMMENDATIONS

Analysis of the VSP data at the MWX well site indicates that the spatial distribution of lenticular-type sands may be delineated by the VSP method. However, the accuracy, limitations, and problems associated with delineating sand bodies were not investigated in this study. To map the spatial distribution of the sand bodies seismically, the following investigations are recommended.

First, perform a detailed three-dimensional model study. A model study can provide important information such as the seismic characters from lenticular-type sand bodies, the accuracy in mapping spatial extent of the body, and the limitations of the seismic method in delineating the sands. Based on model results, the feasibility of the seismic method can be evaluated.

Second, develop a new VSP processing technique to investigate the seismic character changes along the horizontal direction instead of the vertical direction. This processing technique could increase the interpretation capability of the VSP method in delineating lenticular-type sands.

Finally, investigate the optimum field configuration and method in delineating lenticular-type sand bodies at the MWX well site.

REFERENCES CITED

Albright, J. N., Pearson, C. F., and Fehler, M. C., 1980, Transmission of acoustic signals through hydraulic fractures: Society of Petroleum Well Log Analysts, 21st Annual Logging Symposium Transactions.

Balch, A. H., Lee, M. W., Miller, J. J., and Ryder, R. T., 1982, Use of vertical seismic profiles in seismic investigations of the earth: Geophysics, v. 47, no. 6, p. 906-918.

Fried, Jonathan, 1982, written communication, Colorado School of Mines, Golden, Colorado.

Lee, M. W., and Balch, A. H., 1983, Computer processing of vertical seismic profile data: Geophysics, v. 48, no. 3, p. 272-287.

Lorentz, J. C., 1982, Sedimentology of the Mesaverde Formation at Rifle Gap, Colorado and implications for gas-bearing intervals in the subsurface: SAND82-0604, Sandia National Laboratories, Albuquerque, N. M.

Searls, C. A., Lee, M. W., Miller, J. J., Albright, J. N., Fried, Jonathan, and Applegate, J. K., 1983. A coordinated seismic study of the multi-well experiment site: Society of Petroleum Engineers of AIME, SPE/DOE Symposium on low permeability gas reservoirs, Paper no. 11613.